Widespread late Cenozoic increase in erosion rates across the interior of eastern Tibet constrained by detrital low-temperature thermochronometry

Alison R. Duvall,[1,2] Marin K. Clark,[1] Boris Avdeev,[1] Kenneth A. Farley,[3] and Zhengwei Chen[4]

Received 20 June 2011; revised 21 December 2011; accepted 26 April 2012; published 8 June 2012.

[1] New detrital low-temperature thermochronometry provides estimates of long-term erosion rates and the timing of initiation of river incision from across the interior of the Tibetan Plateau. We use the erosion history of this region to evaluate proposed models of orogenic development as well as regional climatic events. Erosion histories of the externally drained portion of the east-central Tibetan Plateau are recorded in modern river sands from major rivers across a transect that spans >750 km and covers a region with no published thermochronometric ages. Individual grains from eight catchments were analyzed for apatite (U-Th)/He and fission track thermochronometry. A wide distribution in ages that, in most cases, spans the entire Cenozoic and Late Mesozoic eras requires a long period of slow or no erosion with a relative increase in erosion rate toward the present. We apply a recently developed methodology for inversion of detrital thermochronometric data for three specified erosion scenarios: constant erosion rate, two-stage erosion history, and three-stage erosion history. Modeling results suggest that rates increase by at least an order of magnitude between 11 and 4 Ma following a period of slow erosion across the studied catchments. Synchroneity in accelerated erosion across the whole of the Tibetan Plateau rather than a spatial or temporal progression challenges the widely held notion that the plateau evolved as a steep, northward-propagating topographic front, or that south to north precipitation gradients exert a primary control on erosion rates. Instead, we suggest that accelerated river incision late in the orogen's history relates to regional-scale uplift that occurred in concert with eastern expansion of the plateau.

Citation: Duvall, A. R., M. K. Clark, B. Avdeev, K. A. Farley, and Z. Chen (2012), Widespread late Cenozoic increase in erosion rates across the interior of eastern Tibet constrained by detrital low-temperature thermochronometry, *Tectonics*, *31*, TC3014, doi:10.1029/2011TC002969.

1. Introduction

[2] Ongoing India-Eurasia continental convergence since ~55–45 Ma [*Rowley*, 1996, 1998; *Zhu et al.*, 2005; *Henderson et al.*, 2010, and references therein] is the widely accepted cause of deformation within Tibet and the surrounding region (Figure 1). The manner in which this convergence is accommodated, however, is controversial. A number of competing mechanisms to explain Cenozoic crustal deformation and surface uplift due to continental collision with India have been proposed. These can be classified broadly into four main categories: (1) underthrusting, (2) rigid block tectonics, (3) continuum models, and (4) crustal flow. Underthrusting of the Indian lithospheric mantle was first suggested by *Argand* [1924]. Adding to this landmark proposal, *Powell* [1986] suggested that wholesale subduction of buoyant Indian continental crust led to underplating and subsequent rise of the Asian Tibetan continental crust. Variations suggest injection [*Zhao and Morgan*, 1987] or underthrusting of Greater Indian crust [*DeCelles et al.*, 2002] or mantle [*Chen et al.*, 2012] into weaker Tibetan lower crust as the mechanism for massive crustal thickening. Recent results from the Hi-CLIMB seismic array do reveal underplating of Indian crust beneath Tibet, however, the northern extent is limited to 31°N, within the Lhasa block [*Nábelek et al.*, 2009]. Rigid block tectonics by lithospheric-scale extrusion and intracontinental subduction resulting in the progressive

[1]Department of Geological Sciences, University of Michigan, Ann Arbor, Michigan, USA.
[2]Now at Cooperative Institute for Research in Environmental Sciences, University of Colorado at Boulder, Boulder, Colorado, USA.
[3]Division of Geological and Planetary Sciences, California Institute of Technology, Pasadena, California, USA.
[4]State Key Laboratory of Earthquake Dynamics, Institute of Geology, CEA, Beijing, China.

Corresponding author: A. R. Duvall, Cooperative Institute for Research in Environmental Sciences, University of Colorado at Boulder, Box 216 UCB, Boulder, CO 80309, USA. (alison.duvall@colorado.edu)

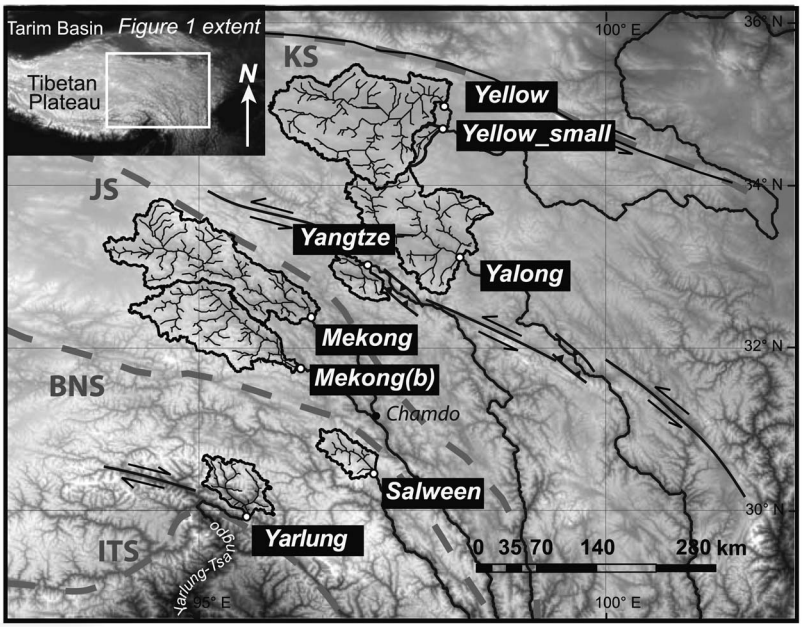

Figure 1. Shaded relief map of study area. Sampled catchments outlined in black; circles represent collection sites of modern river sands. Regional faults are shown in black (simplified from active fault map of *Taylor and Yin* [2009]) and suture boundaries are shown in thicker gray lines: ITS, Indus-Tsangpo suture; BNS, Bangong Nujiang suture; JS, Jingsha suture; KS, Kunlun suture. Inset shows broader Tibetan Plateau region.

northeasterly growth of the plateau [*Tapponnier et al.*, 1982, 2001] were proposed to explain both the great Tibetan crustal thickness as well as widespread strike-slip faulting. In contrast to discrete deformation along rigid blocks, continuum models, such as the thin-viscous sheet [*England and McKenzie*, 1982], describe deformation as distributed through a continuously deforming lithosphere driven by boundary and interior forces. Cenozoic distributed thickening and shortening [*England and Houseman*, 1986, 1989; *Dewey et al.*, 1988] also predicts northward plateau growth, and may have resulted in the removal of mantle lithosphere from beneath Tibet [*Molnar et al.*, 1993]. Others argue for shortening and crustal thickening of Asian lithosphere during the Mesozoic as well as the Cenozoic [*Murphy et al.*, 1997] that resulted in a thick and high southern Tibetan Plateau by Oligocene time [*Kapp et al.*, 2005; *DeCelles et al.*, 2007; *Kapp et al.*, 2007]. Finally, preferential thickening of the lower crust may occur through channel flow [*Bird*, 1991; *Royden et al.*, 1997; *Clark and Royden*, 2000; *Schoenbohm et al.*, 2006; *Royden et al.*, 2008; *Cook and Royden*, 2008], which may be particularly important with respect to the eastward expansion of the plateau.

[3] Temporal records of elevation relate to our mechanical understanding of plateau development because the isostatic response of the continental lithosphere to thickening or reduction in average lithospheric density results in an increase in mean topography. Several attempts to quantify Cenozoic paleoaltimetry from geochemical proxies at various locations within the central Tibetan Plateau suggest that paleoelevations are comparable with modern elevations by at least Miocene time [*Garzione et al.*, 2000; *Rowley et al.*, 2001; *Spicer et al.*, 2003; *Currie et al.*, 2005; *Cyr et al.*, 2005; *Rowley and Currie*, 2006; *DeCelles et al.*, 2007; *Polissar et al.*, 2009]. However, applicability of these results is hindered, at least in part, by limited spatial coverage and large uncertainties (>1000 m) associated with paleoaltimetry techniques [*Quade et al.*, 2011]. Alternatively, plateau-wide erosion histories from the externally drained part of Tibet may be used as a proxy for timing of elevation change [e.g., *Clark et al.*, 2005; *Ouimet et al.*, 2010], because the erosive response predicted from surface uplift and resulting base-level change should also vary among proposed mechanical scenarios. River steepening, channel narrowing, or some combination of both that likely occurs in response to accelerated surface uplift leads to increased fluvial erosion [*Whipple and Tucker*, 1999]. Increased precipitation and storminess [*Reiners et al.*, 2003], incision into weaker rocks, and drainage integration, however, may also lead to accelerated incision irrespective of surface uplift but only if topographic relief preexisted.

[4] Once even moderately high topography (~3000 m) is achieved, the Himalaya and Tibetan Plateau are thought to profoundly influence Asian monsoon processes [e.g., *Prell and Kutzbach*, 1992; *Molnar et al.*, 1993; *An et al.*, 2001; *Molnar*, 2005], which in turn should influence erosion rates. It is commonly thought that the South Asian monsoon results from increased contrast in air temperatures between the high-elevation land surface of Tibet and the surrounding lowlands [*Flohn et al.*, 1968; *Li and Yanai*, 1996; *Yanai and Wu*, 2006] and that tectonic uplift of the Tibetan plateau drives increased monsoon intensity [*An et al.*, 2001; *Molnar et al.*, 1993]. Recent atmospheric records challenge this view because upper-tropospheric (250 hPa) temperatures are highest, not over the Tibetan plateau, but southward over India and Pakistan [*Yanai and Wu*, 2006]. Rather than acting as a heat source, Global Circulation Model (GCM) results

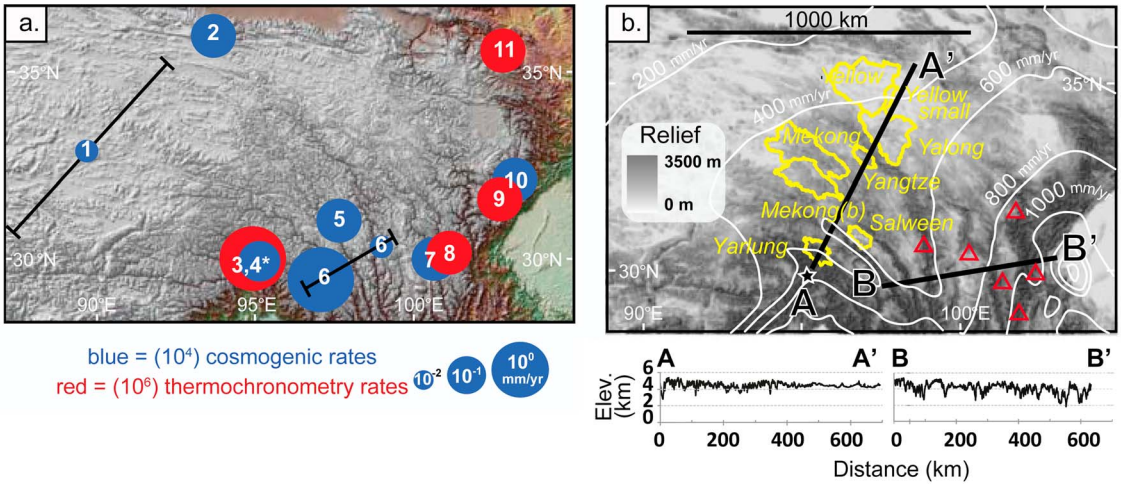

Figure 2. Maps of erosion rate and relief of the central and eastern Tibetan Plateau and perimeter. (a) Reported erosion rates from previous studies. Circles are located at the center of the studied area and are weighted based on reported erosion rates, shown with corresponding number below. Shorter-term rates ($\sim10^4$–10^5 years timescale from cosmogenic radionuclide dating) are in blue and longer-term rates ($\sim10^6$ years timescale from low-temperature thermochronometry) are in red. Asterisk indicates that rates range widely for this location. Note the lack of data for most of the central-east plateau: (1) <0.03 mm/yr [*Lal et al.*, 2004], (2) 0.06–2 mm/yr [*Lal et al.*, 2004], (3) 3–5 mm/yr [*Burg et al.*, 1997, 1998; *Ding et al.*, 2001; *Malloy*, 2004; *Booth et al.*, 2004, 2009; *Zeitler et al.*, 2006; *Seward and Burg*, 2008; *Stewart et al.*, 2008], (4) 0.1–4 mm/yr [*Finnegan et al.*, 2008], (5) 0.1–0.2 mm/yr [*Henck et al.*, 2011], (6) 0.01–8 mm/yr [*Henck et al.*, 2011], (7) ~0.3–0.5 mm/yr [*Ouimet et al.*, 2009], (8) 0.25–0.5 mm/yr [*Clark et al.*, 2005; *Ouimet et al.*, 2010], (9) 0.5–1 mm/yr [*Kirby et al.*, 2002; *Godard et al.*, 2009b], (10) 0.2–0.4 mm/yr [*Godard et al.*, 2009a], (11) 0.2–1 mm/yr [*Jolivet et al.*, 2001; *Zheng et al.*, 2003, 2006, 2010; *Lease et al.*, 2007, 2011; *Clark et al.*, 2010; *Zheng et al.*, 2010]. (b) Relief map generated using a 5 km moving average window over 250 m resolution digital elevation map (downsampled 90 m SRTM data). Topographic profiles of less incised plateau headwaters (A–A′) and more incised eastern plateau perimeter (B–B′). Analyzed catchments are outlined in yellow; previously published bedrock thermochronometry vertical transect locations are shown as red triangles [*Clark et al.*, 2005; *Ouimet et al.*, 2010]. Black star shows start location for the *x* axis of Figure 10 (projected distance line).

demonstrate that high topography surrounding Tibet may be most influential as a barrier to circulation of cool, dry air from the north in the case of the South Asian monsoon [*Boos and Kuang*, 2010] and as a deflector of the jet stream in the case of the "East-Asian monsoon" [*Molnar et al.*, 2010, and references therein], which is actually the head of a midlatitude storm track. Changes in strength and/or duration of these systems may be reflected in the regional erosion record due to the correlation of spatial patterns of erosion with climatic variability across a landscape [e.g., *Montgomery et al.*, 2001; *Reiners et al.*, 2003; *Thiede et al.*, 2004].

[5] Despite the significance of the erosion record on the uplift and climate history of the plateau, relatively little is known about the erosion history of the plateau interior as compared to the more-studied perimeter (Figure 2a). In this study, we determine erosion patterns across the Tibetan Plateau using (U-Th)/He and fission tracks in single-grain detrital apatites (nominal closure temperatures ~55–75°C and ~100–120°C respectively) [*Flowers et al.*, 2009; *Ketcham et al.*, 2007] collected from modern river sands (Figure 1). Detrital studies are best suited for work of this scope because a single sample contains rock materials integrated from a large spatial area. Applying a recently developed inversion approach that derives erosion histories from thermochronometric ages within each catchment [*Avdeev et al.*, 2011], we quantify rates of erosion as well as timing of erosion-rate changes along a NE-SW transect that extends across the entire width of the externally drained portion of the Tibetan Plateau (Figure 1).

2. Erosion Rates Across Tibet From Previous Studies

[6] Short-term erosion rates calculated by measurements of in situ cosmogenic ^{10}Be in quartz from exposed rock surfaces from the internally drained Tibetan plateau interior are low during the late Pleistocene–Holocene (<0.03 mm/yr) with exception of the northern perimeter of the plateau where rates are higher (0.06–2 mm/yr) (Figure 2a) [*Lal et al.*, 2004]. A suite of ^{10}Be detrital data from modern river sands of the Three Rivers Region, SE Tibet (middle reaches of the Salween, Mekong, and Yangtze rivers; Figure 2a) yields estimates of millennial basin-wide average erosion rates that vary from 0.01 to 8 mm/yr across catchments that range from small tributaries (drainage area ~2 km^2) to the main trunk rivers (drainage area >300,000 km^2) [*Henck et al.*, 2011]. Average erosion rates within the upper river reaches (0.1–0.2 mm/yr) are low compared to average rates downstream (0.2–>1 mm/yr). Downstream rates are highest in the western part of the Three Rivers Region where rock-uplift rate is

fastest [*Henck et al.*, 2011]. A similar ^{10}Be detrital study from catchments along the eastern margin of the Tibetan Plateau (Figure 2a) yields basin-averaged erosion rates that range from 0.03 mm/yr to 3 mm/yr, with a catchment average of 0.36 mm/yr and rates of ~0.3–0.5 mm/yr within the trunk rivers [*Ouimet et al.*, 2009]. Rates higher than 0.6 mm/yr occur within the steepest catchments and may be attributed to landsliding. In addition, small basins draining the frontal part of the Longmen Shan yield mean erosion rates of 0.2–0.4 mm/yr (Figure 2a) [*Godard et al.*, 2009a].

[7] Longer-term erosion rates (10^6–10^7 year timescale) relevant to Cenozoic history of tectonic and climate forcing are derived from low-temperature thermochronometry, which records cooling and exhumation from shallow crustal levels (roughly 2–4 km depth). In general, results suggest rates of ~0.1–0.3 mm/yr occurred both in response to local faulting as well as broad regional changes in elevation, although rarely, locally higher rates also occurred (≥1 mm/yr). Across the northern plateau region, apatite fission track (AFT) and apatite helium (AHe) bedrock cooling histories suggest slow cooling through Jurassic and Cretaceous time until at least the early Cenozoic when increases in erosion to rates of ~0.2–1 mm/yr likely occurred in close proximity to mapped faults during Eocene [*Jolivet et al.*, 2001; *Clark et al.*, 2010], Late Oligocene [*Jolivet et al.*, 2001], and mid-to-late Miocene time [*Lease et al.*, 2007, 2011; *Zheng et al.*, 2003, 2006,2010]. Apatite fission track and helium thermochronology from eastern Tibet suggests that a change from slow to rapid cooling occurred during the mid-to-late Miocene along the southeastern and eastern plateau margins [*Arne et al.*, 1997; *Xu and Kamp*, 2000; *Kirby et al.*, 2002; *Clark et al.*, 2005; *Enkelmann et al.*, 2006; *Godard et al.*, 2009b; *Ouimet et al.*, 2010; *Wilson and Fowler*, 2011] (Figure 2). This change in erosion rate is consistent with an erosional response to crustal thickening and broad regional uplift around this time [*Clark et al.*, 2005; *Clark et al.*, 2006; *Wilson and Fowler*, 2011], which is supported by incision of rivers into a relict landscape [*Schoenbohm et al.*, 2004; *Clark et al.*, 2006]. Age/depth data collected along river gorges incised into a low-relief erosion surface reveal slow cooling followed by an increase to rapid erosion rates on the order of 0.25–0.5 mm/yr for the Dadu, Yangtze, and Yalong River gorges between 13 and 9 Ma [*Clark et al.*, 2005; *Ouimet et al.*, 2010] (Figure 2a). Late Cenozoic erosion rates of 0.5–1 mm/yr are also recorded within the Longmen Shan [*Kirby et al.*, 2002] beginning between 10 and 8 Ma [*Godard et al.*, 2009b].

[8] Some of the highest erosion rates in the Himalaya-Tibetan orogenic system lie just south of our sampling transect in the Namche Barwa region at the eastern end of the Himalayan syntaxis (Figure 2a). Comparisons of high- and low-temperature mineral cooling data (^{40}Ar/^{39}Ar hornblende/biotite, U-Pb zircon, (U-Th)/He zircon/apatite, zircon/apatite fission track) from this area show a pattern of very rapid focused exhumation (3–5 mm/yr) since 5 Ma or earlier [*Burg et al.*, 1997, 1998; *Ding et al.*, 2001; *Malloy*, 2004; *Booth et al.*, 2004, 2009; *Zeitler et al.*, 2006; *Seward and Burg*, 2008; *Stewart et al.*, 2008; *Enkelmann et al.*, 2011]. Expansion of the high-exhumation region into the lower Parlung River watershed to the north appears to have occurred since 4 Ma, likely related to growth of a north-plunging antiform [*Seward and Burg*, 2008]. Additionally, short-term basin-wide erosion rates calculated from ^{10}Be analysis range from 0.1–4 mm/yr, with the highest rates corresponding to basins with the greatest relief centered on Namche Barwa [*Finnegan et al.*, 2008]. Studies of Brahmaputra River sediment flux using detrital zircon fission track and U-Pb dating for provenance demonstrate that ~50% of the sediment accumulation in the Brahmaputra system comes from only ~2% of its drainage, which further supports the notion of extreme localization of rapid erosion within this region [*Stewart et al.*, 2008; *Enkelmann et al.*, 2011].

3. Approach and Assumptions

[9] We constrain patterns in long-term erosion across Tibet by first determining detrital apatite helium and fission track ages from modern rivers and then combining these data with basin hypsometries to estimate catchment-wide erosion histories. The ^{4}He concentration in apatite is a function of both production rate and temperature-dependent diffusive loss and the rate of fission track annealing is likewise a function of temperature. Due to relatively low effective closure and annealing temperatures (~55–75°C and ~100–120°C, respectively) [*Gleadow and Duddy*, 1981; *Wolf et al.*, 1996; *Farley*, 2000; *Ketcham et al.*, 2007; *Flowers et al.*, 2009], both alpha particles and fission tracks are appropriate for assessing thermal histories in the shallow crust [*Zeitler et al.*, 1987; *Wolf et al.*, 1996, 1998; *Ehlers and Farley*, 2003]. Closure temperatures vary depending on grain size and cooling rate [*Dodson*, 1973] as well as correlate with effective uranium concentration (eU) due to trapping of helium within radiation-damage sites in the apatite crystal [*Shuster et al.*, 2006; *Flowers et al.*, 2009; *Shuster and Farley*, 2009]. The effect of radiation damage on T_c and thus apatite age is greatest in cases of high eU and is particularly sensitive to the time a sample spends at temperatures below ~90°C [*Shuster et al.*, 2006; *Flowers et al.*, 2007, 2009].

[10] In many cases, thermochronometry ages record the sequential cooling of rocks as they are exhumed toward Earth's surface either by erosive processes or normal faulting. Bedrock elevation transects, which are collections of rocks sampled from incremental elevations over short horizontal distances, are used commonly to calculate apparent exhumation rates from the age-elevation gradients [e.g., *Fitzgerald and Gleadow*, 1990]. The overall shape of the age-elevation profile reflects the thermal history of the samples. An obvious increase in gradient (i.e., a "break in slope") indicates an approximate time of increased exhumation rate. However, in the case of prolonged thermal stability followed by cooling related to exhumation, apparent rates deduced from age gradients are only valid where the total amount of exhumation exceeds the depth to the base of the apatite He or FT partial retention zone [e.g., *Fitzgerald and Gleadow*, 1990]. Thus, this sampling approach is useful in assessing long-term geologic exhumation histories (10^6 Ma) rather than recent events unless those recent events are of large magnitude (>2 km). In cases where enough denudation has occurred to reveal the preserved partial-retention/annealing zone (~2–5 km), then age data along the profile provide the onset timing of the denudation event and give information on denudation rate. Alternatively, ages along a vertical transect within a region that experienced millions of years of slow or

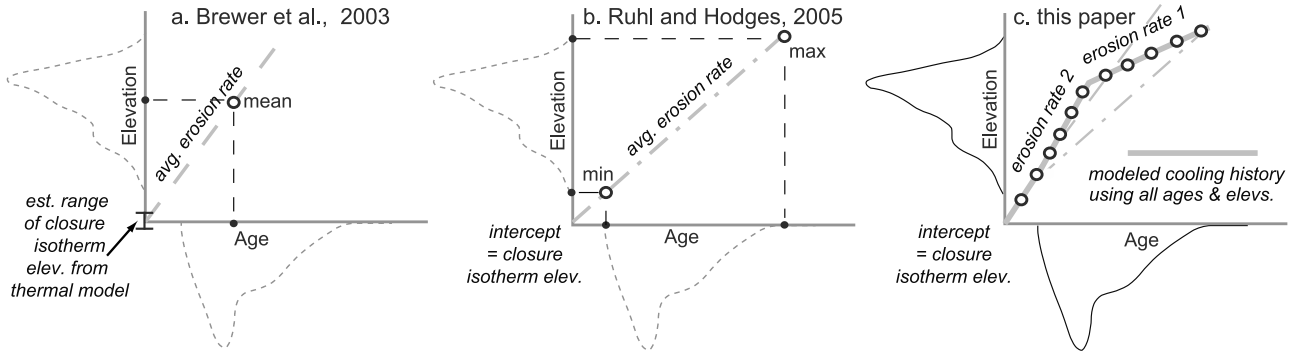

Figure 3. Illustrations showing hypothetical probability density functions (PDFs) of age and elevation to demonstrate different approaches to estimating basin-wide long-term erosion rates. (a) Method of *Brewer et al.* [2003]: average erosion rate (slope of gray dashed line) determined using the catchment mean cooling age and mean elevation (black dots) and a range of closure isotherm elevations estimated from a thermal model. (b) Method of *Ruhl and Hodges* [2005]: average erosion rate (slope of gray dash-dotted line) determined using the catchment minimum and maximum ages and elevations (black dots). The intercept of the line is the estimated isotherm elevation. (c) Method of this paper: catchment wide cooling histories are modeled using an MCMC algorithm to estimate erosion rate (slope of solid gray line) from the entire suite of catchment ages and elevations, allowing for more complicated histories (i.e., breaks in slope) [*Avdeev et al.*, 2011]. Linear segments from Figures 3a (dashed line) and 3b (dash-dotted line) are shown for comparison. The intercept of the line is the estimated isotherm elevation.

no cooling followed by recent and rapid exhumation <~2 km magnitude will largely represent time spent in the partial retention zone. Thus, these data would provide a limit to slow (or null) erosion rates, though would not be useful in determining the more rapid denudation rate of the recent event. In this landscape, we interpret age-elevation relationships to relate to the long-term erosion history of the region.

[11] Poor access and sparse bedrock outcrops preclude sampling bedrock for age/elevation profiles in this study. Instead, we utilize modern river sands collected from single sample sites to measure a suite of ages for each catchment. Catchment-wide erosion histories are evaluated using a recently developed methodology for interpreting detrital thermochronometry data [*Avdeev et al.*, 2011]. Several assumptions are inherent to this approach. We relate thermochronometry ages to the cooling history of rocks as they move toward the surface by erosion rather than due to cooling of volcanics or shallowly emplaced plutons or exhumation by normal faulting. Our model results are estimated assuming piecewise linear age-elevation relationships, just as in a bedrock sampling approach. We derive apparent erosion history assuming vertical advection, a flat closure isotherm, and constant geothermal gradient and surface temperature through time. We also assume that sediment is not stored for significant periods of time ($\leq 10^5$ years) within catchments and that erosion rates as well as apatite concentrations in bedrock are spatially uniform.

[12] Catchments without major mapped Cenozoic fault systems (Figure 1) were targeted for sampling because we are interested in erosion related to regional processes rather than to local deformation. However, it is possible that unmapped structures and minor splays may be present within our catchments. Topography has been shown to influence the interpretation of erosion rates from the age/elevation relationship, both by warping of isotherms in the shallow crust and by the effect of cooling rate on the effective closure temperature [e.g., *Stüwe et al.*, 1994; *Mancktelow and Grasemann*, 1997; *Braun*, 2002; *Ehlers and Farley*, 2003; *Reiners and Brandon*, 2006]. Therefore, we consider the estimated erosion rates in this study to be apparent and recognize these values may overestimate real long-term rates if significant advection of the isotherms has occurred. However, we note that relief within catchments on the high plateau (generally 1000–2000 m) is focused in trunk rivers, effectively creating short-wavelength topography and therefore the closure isotherms should be relatively flat [*Braun*, 2002]. Regional geologic mapping [*Pan et al.*, 2004] shows widespread occurrence of rock types known to contain apatite, which diminishes the potential for point sources. Moreover, recent cosmogenic radionuclide (CRN) studies show that sampling larger catchments (>100 km^2 drainage area) for longer-term erosion rates (10^6 years), as we do here, likely averages out temporal and spatial point sources related to sediment flux from isolated landsliding events [*Niemi et al.*, 2005; *Yanites et al.*, 2009].

[13] In previous detrital-thermochronometry studies, time-averaged catchment-wide erosion rates were calculated either by differencing the oldest and youngest ages and the lowest and highest elevations within the catchment [*Ruhl and Hodges*, 2005] or by using the mean age and elevation within the catchment along with an estimated elevation of the closure isotherm determined from a thermal model [*Brewer et al.*, 2003] (Figure 3). The principal limitation in these approaches is the assumption of steady state erosion histories. In contrast, our approach allows estimation of time-varying thermal histories by using the distribution of elevation and age data from each catchment [*Avdeev et al.*, 2011] (Figure 3). We aim to find the simplest geologically reasonable erosion histories that adequately explain the data for each catchment beginning with assessment of constant erosion rate through time. Scenarios with zero or more changes in rate through time were considered until additional erosion-

Table 1. Catchment Geomorphology

Catchment Name	Drainage Area (km^2)	Min. Elev. (m)	Max. Elev. (m)	Elev. Range (m)	Mean Elev. (m)	Mean Slope (deg)
Tsangpo	3520	2750	6184	3434	4535	24.9
Salween	2401	4318	5646	1328	4799	13.6
Mekong(b)	11150	3663	5682	2019	4751	16.3
Mekong	15869	3748	5796	2048	4681	14.6
Yangtze	2210	3684	5461	1777	4475	16.9
Yalong	14011	3980	5208	1228	4536	8.6
Yellow	19170	4219	5219	1000	4507	3.8
Yellow_small	998	4217	5174	957	4502	4.9

rate changes did not result in a noticeably better fit with the data. We recognize that more complicated alternative histories with spatially varying erosion and non-vertical pathways not considered here might also be permissible.

4. Sampled Catchments

[14] We collected detrital samples from modern headwater rivers along a NE-SW transect that spans >750 km within the externally drained east-central plateau (Figure 1). Catchments along this transect include seven larger basins (drainage area 2000 to 20000 km^2): the Yellow, Yalong, Yangtze, Mekong and Mekong(b) (both part of the Mekong River watershed), Salween, and the Parlung tributary to the Tsangpo-Yarlung, referred to here after simply as Yarlung, and one smaller basin (1000 km^2), Yellow_small, which is a tributary of the Yellow River (Table 1 and Figure 1). The hypsometry (relation between area and elevation) and landscape characteristics (mean/min/max elevation and relief measured by subtracting the highest and lowest elevations within each catchment) for each catchment were estimated using 90 m resolution SRTM digital elevation data and are shown in Table 1. Mean elevation (∼4600 m) and mean catchment relief (∼1500 m) are similar within the studied river basins, with exception to the high-relief, glaciated Yarlung catchment (mean catchment relief of ∼3500 m) (Figure 2b and Table 1). Mean slope angle decreases from south to north, with lowest average slopes (<10°) in the Yellow and Yalong catchments, middle average slopes (∼15°) in the Yangtze, Mekong, Mekong(b) and Salween catchments, and highest average slopes (∼25°) in the Yarlung catchment (Table 1). The high plateau in the vicinity of our sampled catchments is generally arid with a north to south increase in average annual precipitation (∼300 mm/yr within the northern catchments and ∼600 mm/yr within the southern catchments) [*New et al.*, 2002; K. Matsuura and C. Willmott, Terrestrial Air Temperature and Precipitation: 1900–2006 Gridded Monthly Time Series, version 1.01, online data, 2007, available at http://climate.geog.udel.edu/∼climate/]. In contrast, the surrounding regions to our study area to the south and east are wetter with average annual precipitation as much as 1100–1500 mm/yr [*New et al.*, 2002] and have greater local relief (Figure 2b).

[15] Study-area catchments include mapped geologic units of variable age and rock type [*Pan et al.*, 2004] (Figure 4). Paleozoic rocks are predominantly sedimentary, including shale, limestone, sandstone, and conglomerate, with minor amounts of slate, schist, marble, and volcanics. Mesozoic rocks are mainly Triassic marine facies mudstone, siltstone, limestone, and sandstone known collectively as the Songpan-Ganzi turbidite complex [*Weislogel*, 2008], Jurassic continental clastic rocks, and granitoids (granite, granodiorite, quartz diorite) that are known to contain apatite from previous studies [*Xu and Kamp*, 2000; *Wilson and Fowler*, 2011]. Cenozoic rocks are less abundant within the study area as we purposefully avoided sampling catchments with large volumes of mapped sedimentary or igneous rocks from this time period to assure minimal sediment storage and that cooling relates to erosion. U-Pb ages measured from detrital zircons from two of the sampled catchments are older than Cenozoic age (see Table S3), which supports our assumption that minerals from Cenozoic volcanic rocks or shallowly emplaced plutons were avoided.[1] Quaternary deposits, mostly fluvial, are present mainly in small volume within all studied catchments.

5. Methods

[16] River sands were collected from sandbars within the active channel during the early winter months when river levels were low. To ensure a well-mixed population of material from each catchment, each ∼5 kg sample was compiled from multiple smaller aliquots spaced a few meters apart [*DeGraaff-Surpless et al.*, 2003; *Lease et al.*, 2007]. Samples were sieved (Standard #18 1,000 μm mesh sieve), washed in de-ionized water and dried in an oven at low temperatures (40°C) then further separated by grain size using a U.S. Standard #60 250 μm mesh sieve. Apatite and zircon separates were derived from these <250 μm aliquots by exploiting density and magnetic susceptibility differences.

5.1. Apatite (U-Th)/He Dating (AHe)

[17] Individual apatite grains were handpicked at the University of Michigan and analyzed for (U-Th)/He ages at the Noble Gas Laboratory at Caltech with ∼20 single-grain analyses for each sample (135 total grains analyzed; Table S1). To avoid additional bias, we selected grains of varying morphology rather than preferentially picking only euhedral, unbroken grains as is common in bedrock studies. In many catchments, this resulted in morphologies that range from pristine to rounded (Figure 5) but all grains were selected to have minimal visible inclusions using a Leica MZ16 stereozoom microscope under cross polarization at 160× magnification. Single grains were loaded into a platinum packet and laser heated in a vacuum to 1025°C for five minutes to release all helium. Helium was measured in a quadrupole mass spectrometer using ^{3}He isotope dilution.

[1] Auxiliary materials are available in the HTML. doi:10.1029/2011TC002969.

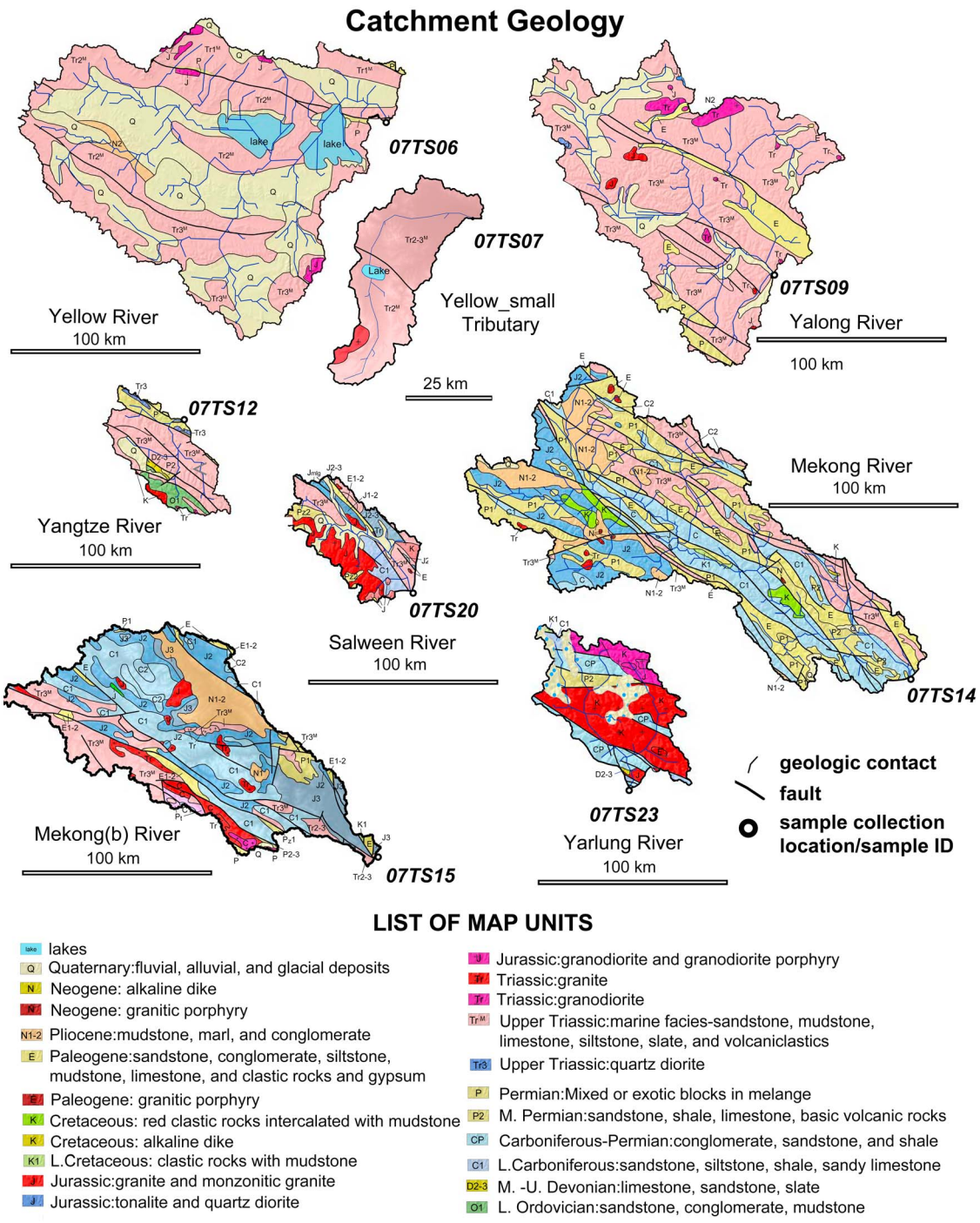

Figure 4. Generalized geologic maps of studied catchments (simplified from 1:1,500,000 geologic map [*Pan et al.*, 2004]). (a) Yellow catchment, (b) Yellow_small catchment, (c) Yalong catchment, (d) Yangtze catchment, (e) Mekong catchment, (f) Salween catchment, (g) Yarlung catchment, (h) Mekong(b) catchment.

After initial degassing, samples were reheated to ensure complete release of helium. Analyses that yield helium upon a second reheating step ("re-extract") likely contain inclusion(s) of a different radiogenic mineral phase, such as zircon. In this study, no samples yielded significant re-extraction of gas during this step. After gas extraction, each grain was placed in HNO_3, spiked with ^{235}U and ^{230}Th and heated to 95°C for one hour to facilitate complete dissolution. The solution was analyzed on an inductively coupled plasma mass spectrometer (ICP-MS) for uranium and thorium content. Raw and "corrected" ages were calculated for each replicate. The alpha-ejection correction (F_T) is based on the measured size of the grain and is applied to correct for ^4He ejected from the grain due to the long distance (~20 μm) that alpha particles travel during production [*Farley et al.*, 1996]. Apatite grains in this study

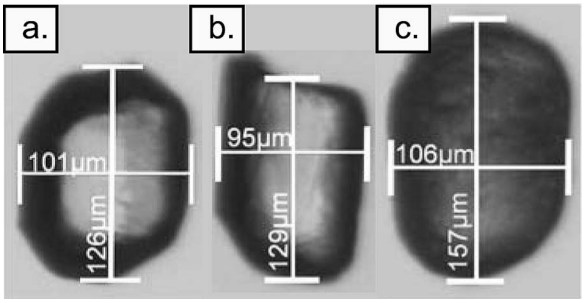

Figure 5. Digital images of typical apatite grains selected for helium analysis in this study. Grains categorized into three classes: (a) "pristine," (b) "average," and (c) "rounded." See text for details.

ranged from 40 μm to 75 μm in prism half-width and F_T values ranged from 0.61 to 0.8 (Table 2). Grain abrasion during transport has been shown to complicate alpha-ejection correction in detrital apatite helium studies [*Rahl et al.*, 2003], which we considered when calculating corrected ages (see section 6.1).

5.2. Apatite Fission Track (AFT)

[18] Apatite fission track ages were determined for six of the larger catchments and the one small catchment by Apatite to Zircon, Inc. [*Donelick et al.*, 2005], with ~40 single grains analyzed per sample (275 total grains analyzed; Table S2). Natural fission tracks were revealed by immersing polished apatite grain mounts in 5.5N HNO_3 for 20 s (±0.5 s) at 21°C (±1°C). Grain mounts were then irradiated with $\sim 10^7$ tracks/cm^2 from a ^{252}Cf source in a vacuum chamber in order to measure horizontal, confined tracks, and track lengths. Fission track ages were determined using a modified decay equation that includes calibration for the LA-ICP-MS using the Durango fluorapatite standard (fission track age of 30.6 Ma) [*Donelick et al.*, 2005]. The discrete nature of tracks formed by spontaneous fission biases the age estimate for grains with zero to few counts. This is less of an issue in bedrock studies that typically report an average of 20–40 single grain ages or a pooled age, which is calculated from the sum of spontaneous counts divided by the sum of induced counts for all grains analyzed per sample. However, in our detrital approach, we rely on every individual age and therefore apply a 1/2 track correction in calculating ages, which has negligible effect for grains with large counts [*Galbraith*, 2005]. The average difference between the ages calculated with and without the track correction is less than 10% among the 275 grains analyzed (Table S2).

5.3. Inverse Detrital Erosion Models

[19] We jointly model AHe and AFT data for each catchment using a Bayesian estimation technique [*Avdeev et al.*, 2011] (http://code.google.com/p/thermochron/) to estimate specified erosion models that, in some cases, allow for changes in spatially uniform erosion rate through time. Estimates of free model parameters, which are erosion rate (e_i in km/My), age of change in erosion rate (α_{br} in My), and modern elevation of the closure isotherm (h_c in km), were obtained (see auxiliary material and *Avdeev et al.* [2011] for further method details). All inversion models in this study are based on the following likelihood function that defines the probability of the observed detrital data given values of model parameters and hypsometry

$$p_d(\alpha) = \iint_W p_b(h(w), \alpha) dw \tag{1}$$

where p_d is the probability density of observing a detrital grain with age α and is an integral of the probability of observing this age in bedrock p_b over a watershed W where elevations $h(w)$ are defined by a digital elevation model. The probability of observing a bedrock age a at the catchment surface is defined by $\bar{b}$ and its measurement error (s) where $\bar{b}$ is a function of the exhumation history of the catchment. We assume that measurement error has a normal distribution with a mean equal to the true age and a standard deviation σ, thus

$$p_b(h, a) = 1/\sqrt{2\pi\sigma} \exp\left(-\frac{1}{2} \left(\frac{a - \bar{b}(h)}{\sigma} \right)^2 \right). \tag{2}$$

[20] Because we assume a vertical exhumation pathway and a flat closure isotherm, bedrock cooling ages are invariant in the horizontal direction and thus a function only of elevation. We rely on approximately twenty individual age analyses per each catchment and estimate average standard deviation from AHe bedrock age replicates reported previously from bedrock data in northeastern Tibet [*Clark et al.*, 2010], eastern Tibet [*Kirby et al.*, 2002] and southeastern Tibet [*Clark et al.*, 2005; *Ouimet et al.*, 2010] and use it as the uncertainty on detrital ages (22% of age, 1σ std. dev.). Error estimation for single fission track ages is problematic, especially for grains with low track counts [*Galbraith*, 2005]. We estimate error

Table 2. Detrital Thermochronometry Age Summary

Catchment	N_{AHe}[a]	AHe Age Range (Ma)	N_{AFT}[b]	AFT Age Range (Ma)	Elevation Range (m)	Mean Elevation (m)
Tsangpo	19	1.17–14.29	40	1.33–44.46	2750–6184	4535
Salween	20	25.2–145.12	40	13.21–145.99	4318–5646	4799
Mekong(b)	10	9.98–57.12	0	—	3663–5682	4681
Mekong	20	9–76.4	40	9.32–224.27	3748–5796	4751
Yangtze	20	3.93–72.69	40	3.01–264.66	3684–5461	4475
Yalong	19	12.57–143.92	40	5.42–163.29	3980–5208	4536
Yellow	20	4.32–160.22	40	16.24–238.30	4219–5219	4507
Yellow_small	17	32.11–203.73	35	21.66–277.91	4217–5174	4502

[a]Number of apatite grains analyzed for (U-Th)/He.
[b]Number of apatite grains analyzed for fission track.

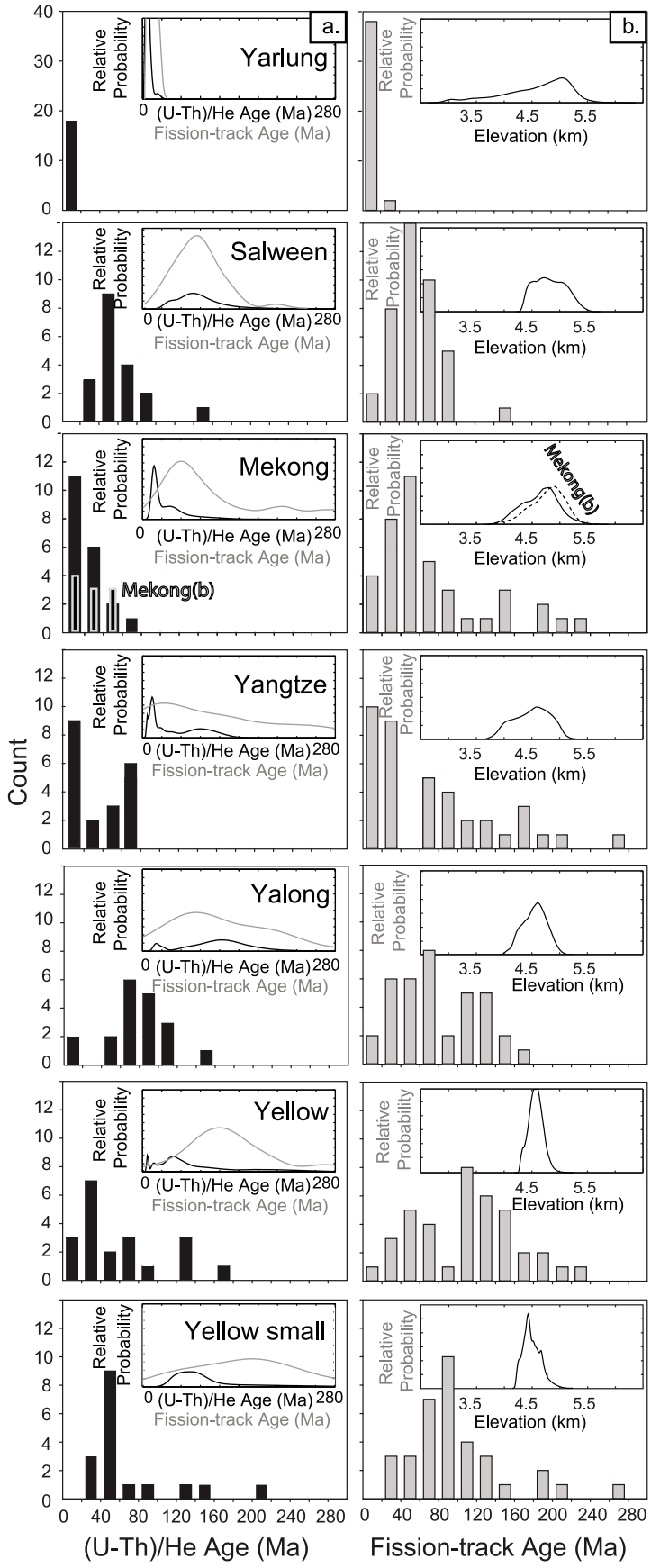
a.
b.
Yarlung
Salween
Mekong
Mekong(b)
Yangtze
Yalong
Yellow
Yellow small
Relative Probability
Count
(U-Th)/He Age (Ma)
Fission-track Age (Ma)
Elevation (km)
0 40 80 120 160 200 240 280
3.5 4.5 5.5

Figure 6

along with other model parameters assuming that it is proportional to the true fission track age ($\sigma = s\bar{b}$) [*Avdeev et al.*, 2011].

[21] Each model specifies priors, which are probability distributions of model parameters that express prior knowledge. Soft data inputs of this type eliminate unrealistic model results (e.g., closure isotherm elevations at or above the Earth's surface, or unreasonably high erosion rates). In this study, priors for erosion rate in all cases were set uniform between 0 mm/yr to 1 mm/yr, which encompasses a wide range of reasonable erosion rates for high-elevation plateaus such as Tibet. Priors for the age(s) of erosion-rate change(s) (i.e., "break in slope") were set uniform between 0 Ma to 65 Ma, allowing for rate change(s) at any time during the Cenozoic Era. Finally, the priors for the closure isotherm elevation were assigned as a truncated normal distribution about a mean value, which was calculated on a per-catchment basis by subtracting 2.2 km and 3.7 km from the average elevation within the sampled catchment for AHe and AFT respectively. These closure isotherm depths are based on geothermal gradients across the sampling transect of 20–35°C/km determined from heat-flow measurements [*Hu et al.*, 2000] in combination with appropriate ranges in effective closure temperatures of helium in apatite of 55–75°C, predicted by the RDAMM model [*Flowers et al.*, 2009] assuming cooling rates, eU, and grain sizes reasonable for this study, and fission track annealing temperatures of 100–120°C [*Ketcham et al.*, 2007].

6. Results

6.1. Detrital Cooling Ages

[22] The catchments have widely distributed apatite helium and fission track ages that span the entire Cenozoic and into the Mesozoic eras and mean basin-wide elevations of ~4600 m (Table 2 and Figure 6), with the exception of the Yarlung. Cooling-age distributions from the Yarlung catchment are more limited, with no AHe ages older than mid-Miocene or AFT ages older than Eocene (Table 2 and Figure 6). Although the Salween and Yellow_small catchments have broadly ranging age populations that include Mesozoic ages, they have no AHe or AFT ages younger than Miocene (Table 2 and Figure 6).

[23] Apatite grain quality varies across the sampled catchments from pristine to rounded (Figure 5), yet there is no strong correlation between grain morphology and corrected helium age and all morphology types yield ages that span the Cenozoic era (see Figure S1 in the auxiliary material). Detrital helium results are potentially complicated by the partial or entire loss of the He depleted rim of apatite due to abrasion during transport. Abrasion may alter crystal shape such that the analyzed and original grain shapes are significantly different, thereby complicating the Ft correction [*Rahl et al.*, 2003]. The majority of uncorrected AHe ages (Table 2) are younger than the depositional age of most sedimentary units (Paleozoic and early Mesozoic) mapped throughout the study area [*Pan et al.*, 2004], which suggests that rocks were buried and heated after sedimentary deposition to temperatures greater than 70°C. Additionally, a strong positive correlation between grain quality and area of mapped sedimentary and plutonic units within catchments suggests that the majority of the rounding/clouding in highly weathered grains probably occurred before deposition in pre-Cenozoic sedimentary basins that were later heated then exhumed rather than from more recent weathering and river transport. Because grains are likely reset with respect to the AHe system, we apply the full alpha-ejection correction to all analyses.

6.2. Modeled Erosion Histories

[24] We jointly inverted AHe and AFT data for each individual catchment assuming three erosion scenarios: (1) constant erosion rate through time (2) two distinct erosion rates in time and (3) three distinct erosion rates in time. We found that including more than three distinct periods of erosion did not provide additional information (i.e., additional periods produced similar erosion rates). The fit of models to data is evaluated by comparing cumulative probability distribution from the actual samples to those of synthetic samples generated from model parameters using a goodness-of-fit plot [*Avdeev et al.*, 2011]. All reasonable models should produce synthetic data that are similar to observed data; therefore, overlap of the two sample suites indicates an acceptable model fit. Inability to find reasonable fits for proposed models likely invalidates the tested erosion history or model assumptions. Model estimates of erosion rates over various intervals and timing of rate changes for all catchments individually are reported as 95% confidence intervals (Table 3).

6.2.1. Constant Erosion Rate Through Time

[25] Initially, we constrain a constant exhumation model assuming that erosion rate does not change through time within the catchments. In this scenario, bedrock ages ($\bar{b}(w)$ in equation (2)) are described by a piecewise linear function of elevation with one segment:

$$\bar{b}(h_c) = h_c/e \tag{3}$$

where e is the slope. Model results are displayed as a series of plots (Figures 7–9 and Figures S2–S4). Figures 7a, 8a, and 9a show cooling pathways predicted for AHe (blue lines) and AFT (green lines) plotted on a graph of age versus elevation. Figures 7b, 8b, and 9b are a cumulative probability density plot displaying the observed AHe (blue dots) and AFT (green dots) detrital ages and synthetic data (gray band) generated using results of predicted model parameters. Model fidelity is judged by visual comparison of the observed data and simulated data, with high degree of overlap between the dots and the swath indicating an acceptable model fit. Figures 7c, 7d, 8c, 8d, 9c, and 9d show

Figure 6. Sampled catchment thermochronometric ages and hypsometry. (a) Histogram plots of (U-Th)/He for each studied catchment, south to north. Note the different scale of the *y* axis for the Yarlung catchment. Insets show PDFs of (U-Th/He) ages in black and fission track ages in gray constructed using kernel density estimation. (b) Histogram plots of fission track results. Insets show catchment hypsometry (frequency distributions of elevation). Mekong(b) (U-Th)He ages and hypsometry are displayed within the Mekong panel. No fission track ages were measured for this catchment.

Table 3. Model Results Summary: Catchments Modeled Independently

Two-Stage Erosion History												
		Joint Inversion			AHe Only			AFT Only				
Catchment	a_{br} (Ma)	e_1 (mm/yr)	e_2 (mm/yr)	a_{br}	e_1	e_2	a_{br}	e_1	e_2
Tsangpo	4–9	0.01–0.14	0.38–0.67	0.5–55	0.004–0.91	0.258–0.691	4–12	0.003–0.141	0.315–0.86
Salween	3–61	0.003–0.03	0.05–0.73	1–58	0.003–0.024	0.03–0.75	3–60	0.01–0.93	0.0002–0.324
Mekong(b)	—	—	—	1–20	0.006–0.038	0.06–0.67	—	—	—
Mekong	10–14	0.006–0.01	0.18–0.29	10–15	0.005–0.17	0.12–0.27	5–51	0.002–0.009	0.054–0.41
Yalong	3–24	0.003–0.005	0.06–0.72	0–30	0.003–0.029	0.0007–0.825	43–60	0.001–0.002	0.053–0.104
Yellow	3–8	0.003–0.005	0.35–0.97	2–10	0.002–0.005	0.138–0.918	0–56	0.008–0.063	0.0002–0.712
Yellow_small	4–58	0.003–0.009	0.05–0.49	8–60	0.001–0.008	0.03–0.23	0–57	0.006–0.08	0.0001–0.782

Three-Stage Erosion History														
	Joint Inversion					AHe Only				AFT Only				
Catchment	a_{br1}	a_{br2}	e_1	e_2	e_3	a_{br1}	a_{br2}	e_1	e_2	e_3	a_{br1}	a_{br2}	e_1	e_2	e_3
Yangtze[a]	54–60	6–12	0.001–0.002	0.08–0.18	0.21–0.44	25–60	7–13	0.005–0.95	0.0001–0.015	0.122–0.350	16–55	0–21	0.0007–0.002	0.0003–0.805	0.0001–0.690

[a]Two breaks in slope model preferred. Joint inversion single break model. See Figure S2.

the relative probability of predicted erosion rate and closure isotherm elevation for AHe (blue) and AFT (green). Model runs that include changes in erosion rate (Figures 8e and 9e) show the relative probability of the timing of the rate change(s).

[26] Strong mismatch between predicted synthetic data and observed data suggests that the constant erosion model is unsuitable for all of the catchments with two exceptions in the southern part of our study area (Figure 7). The Yarlung catchment is reasonably well described by a constant erosion rate of 0.28–0.41 mm/yr. The goodness-of-fit plot for the Salween catchment also shows that these data are reasonably fit by a constant erosion rate model with an erosion rate of 0.04–0.06 mm/yr (Table 3).

6.2.2. Two-Stage Erosion History

[27] Next we assume a two-stage exhumation model assuming bedrock ages are described by a piecewise linear function of elevation with two segments:

$$\begin{matrix} \bar{b}(h_c) = (h_c - h_{c1})/e_1, \bar{b} > a_{br} \\ (h_c - h_{c2})/e_2, \bar{b} < a_{br} \end{matrix} \quad (4)$$

where e_i is the slope and h_{ci} is the intercept of each segment and α_{br} is the age of the break in slope. Goodness-of-fit plots show that an erosion history with an increase in erosion rate is reasonable for all of the catchments (Figure 8b). Although the constant erosion rate model provided a reasonable fit to the Yarlung and Salween data, adding a break in slope results in a better fit to the oldest ages in these samples, thus we prefer a two-stage model for these catchments. Assuming a single break in slope occurred, four of the catchments (Yarlung, Mekong, Yangtze, and Yellow) have relatively narrow probability peaks for the timing of erosion-rate change suggesting that the erosion rate, which was slow (0.003–0.01 mm/yr), increased at least an order of magnitude (0.1–1 mm/yr) sometime between 17 and 4 Ma (Figure 8 and Table 3). The Yalong River shows an increase in erosion rate from 0.003 to 0.005 mm/yr to 0.06–0.72 mm/yr between 24 and 3 Ma. The change in erosion rates from 0.003 to 0.03 mm/yr to 0.05–0.73 mm/yr and 0.003–0.009 mm/yr to 0.05–0.49 mm/yr for the Salween and Yellow_small catchments are less precisely constrained between 61 and 3 and 58–4 Ma respectively.

6.2.3. Three-Stage Erosion History

[28] Bedrock ages described by a piecewise linear function of elevation with three segments (i.e., two breaks in slope) can be expressed as:

$$\begin{matrix} \bar{b}(h_c) = (h_c - h_{c1})/e_1, \bar{b} > a_{br1} \\ (h_c - h_{c2})/e_2, \bar{b} < a_{br1} > a_{br2} \\ (h_c - h_{c3})/e_3, \bar{b} < a_{br2} \end{matrix} \quad (5)$$

With one exception (Yangtze), results from this model do not show significant improvement in goodness of fit from two-stage models and relative probabilities of timing of the first and second breaks in slope overlap (Figure S2). In the Yalong case, precision on the timing of rate changes is reduced as the window of ages within the 95% confidence interval spans almost the entire Cenozoic. For these reasons, we prefer the two-stage erosion rate models for all catchments except for

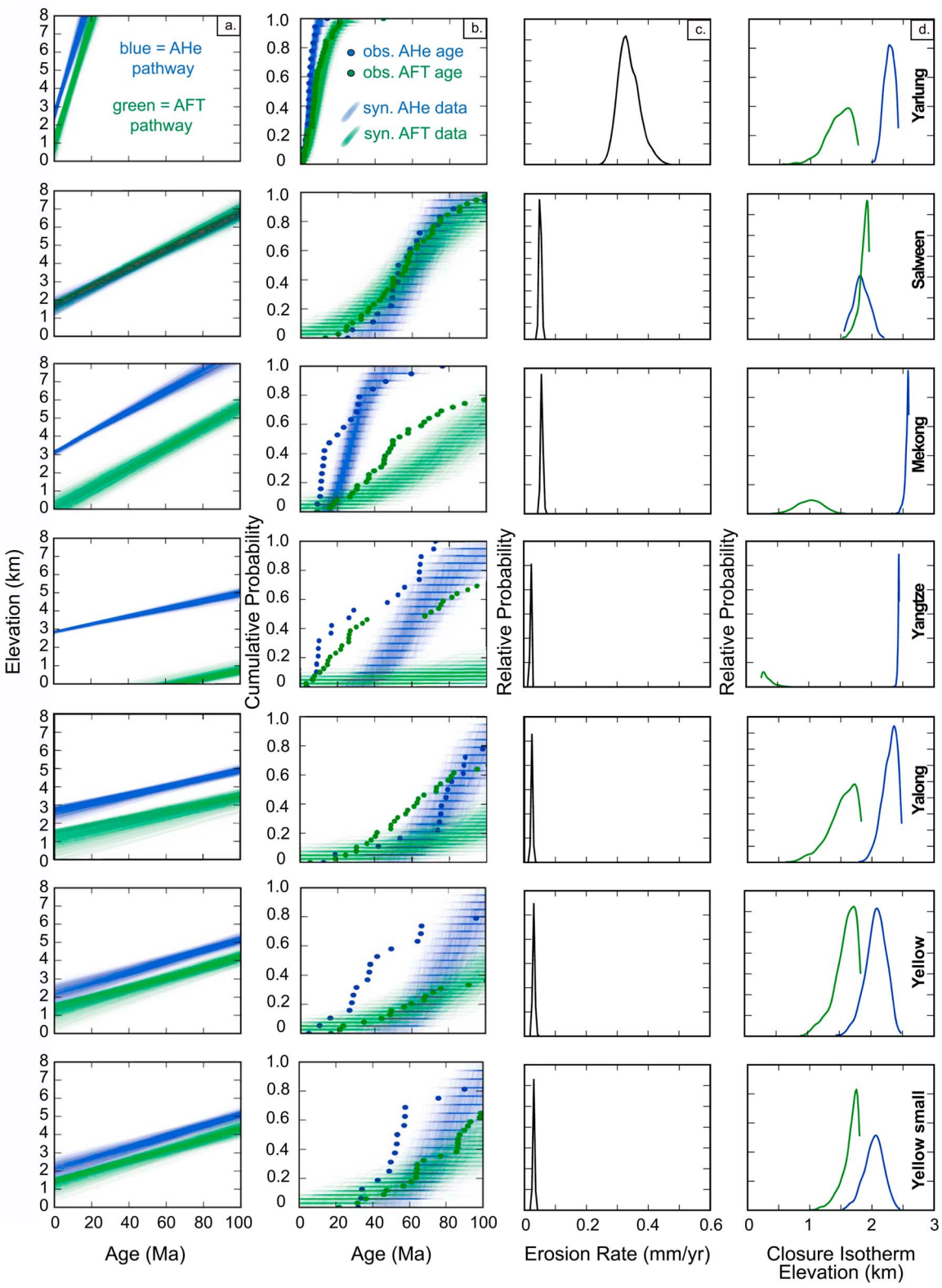

Figure 7. Model results of joint AHe and AFT inversion assuming a constant erosion rate through time. (a) Plots of age (Ma) against elevation (km); blue lines represent AHe cooling pathways and green lines represent AFT cooling pathways. (b) "Goodness of Fit" plots: cumulative probability density plots showing actual AHe (blue dots) and AFT (green dots) ages and swaths of synthetic AHe (blue) and AFT (green) data. Because reasonable models should produce synthetic data that are similar to observed data, overlap of the two sample suites indicates an acceptable model fit. (c) Relative probability of erosion rate (mm/yr). (d) Relative probability of closure isotherm elevation (km) for AHe (blue) and AFT (green).

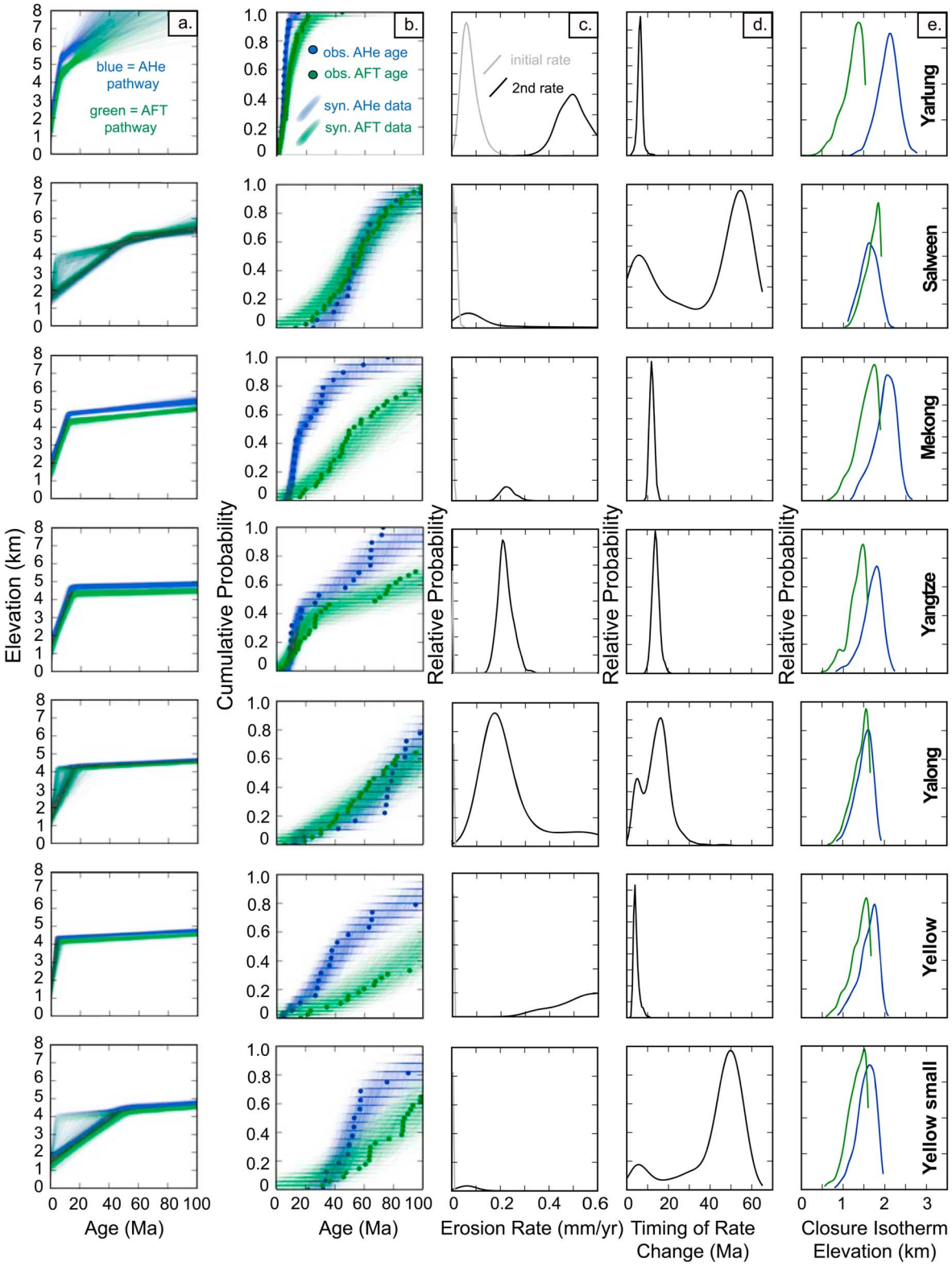

Figure 8. Model results of joint AHe and AFT inversion assuming one discrete change in erosion rate through time. (a) Plots of age (Ma) against elevation (km), blue lines represent AHe cooling pathways and green lines represent AFT cooling pathways. (b) "Goodness of Fit" plots: cumulative probability density plots showing actual AHe (blue dots) and AFT (green dots) ages and swaths of synthetic AHe (blue) and AFT (green) data. (c) Relative probability of erosion rate (mm/yr). Initial erosion rate is shown as light gray line and post-change erosion rate is shown in black. (d) Relative probability of timing of erosion rate change (Ma). (e) Relative probability of closure isotherm elevation (km) for AHe (blue) and AFT (green).

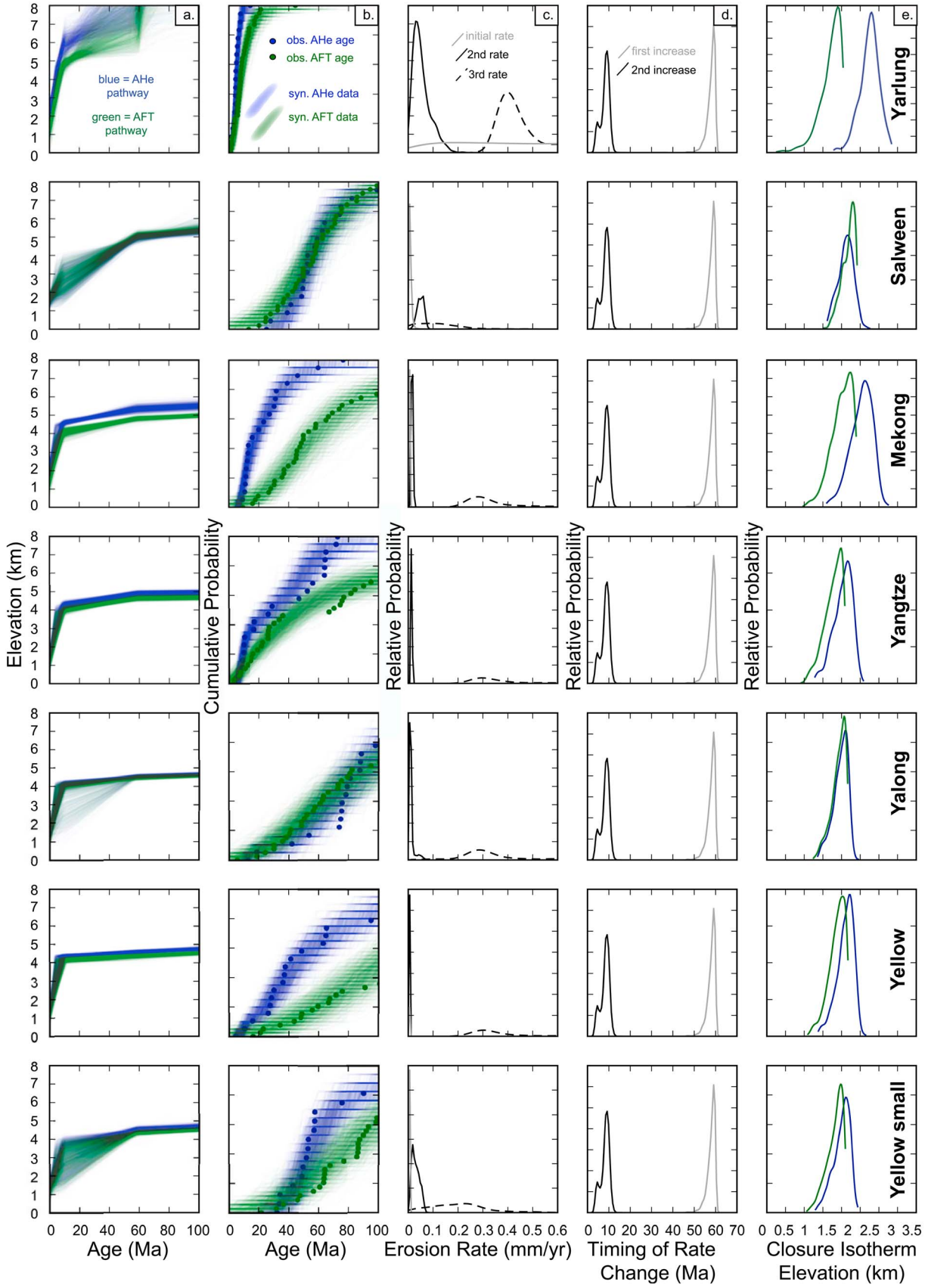

Figure 9. Model results of inversion using all of the data assuming that catchments share a common erosion history. Same panels as in Figure 8.

Table 4. Model Results Summary: Common Erosion History Model[a]

Catchment	a_{br1}	a_{br2}	e_1	e_2	e_3
Tsangpo	54–60	4–11	0.05–1	0.002–0.12	0.33–0.67
Salween	54–60	4–11	0.0005–0.27	0.02–0.07	0.002–0.02
Mekong	54–60	4–11	0.002–0.007	0.009–0.02	0.2–0.58
Yangtze	54–60	4–11	0.0006–0.001	0.01–0.02	0.23–0.63
Yalong	54–60	4–11	0.002–0.004	0.004–0.04	0.08–0.63
Yellow	54–60	4–11	0.002–0.005	0.002–0.007	0.22–0.67
Yellow_small	54–60	4–11	0.002–0.006	0.008–0.06	0.002–0.4

[a]Age of first erosion rate change, a_{br1}; age of second erosion rate change, a_{br2}; earliest erosion rate, e_1; erosion rate after first change, e_2; erosion rate after second change, e_3.

the Yangtze. The Yangtze catchment data is well fit by a three-stage erosion history with an initial increase in erosion rate from 0.001 to 0.002 mm/yr to 0.08–0.18 mm/yr at 60–54 Ma followed by a second and larger increase to erosion rates of 0.21–0.44 mm/yr at 12–6 Ma (Table 3).

6.2.4. Common Erosion History Among Catchments

[29] The overlap in timing (late Miocene to early Pliocene) of an increase in erosion rates shown by individual catchment models suggests a relatively synchronous erosion history across the sampling transect. In order to assess this hypothesis, we considered all of the data together in a single model. Essentially, a larger data set may allow us to more precisely constrain the timing of rate change. The common erosion model assumes that all catchments experienced an increase in erosion rate at the same time and allows for three linear segments, the most flexible model that was found prior. Model results show reasonable fits to data with an increase in erosion rate across all catchments at 11–4 Ma (95% confidence; Figure 9 and Table 4). Results also show an earlier change in erosion rate at 60–54 Ma (95% confidence; Figure 9 and Table 4). The goodness-of-fit plots demonstrate that this erosion history is permissible for all of the catchments. However, because only the Yangtze catchment showed two distinct peaks in timing of erosion rate increase in individual modeling (at 60–54 Ma and 12–6 Ma; see section 6.2.3), the timing of the initial break in slope for the common erosion model may be weighted by this catchment.

6.3. Comparison of Joint Versus Independent AHe and AFT Inversions

[30] In theory, analysis of minerals from the same sample with multiple thermochronometers should resolve consistent erosion histories when modeled independently, though AFT and AHe data will be most sensitive to older and younger erosion events respectively due to differences in closure temperature. For comparison, we present results of independent AHe and AFT inversion models assuming one discrete change in erosion rate in time (Table 3; see Figures S3 and S4). In general, the independent AHe and AFT models are compatible with one another and with a late Cenozoic increase in erosion rate interpreted from joint inversions using both thermochronometers (Figure 8). Joint inversions increase the precision of estimated parameters compared to models using AHe or AFT data independently (Table 3), and more importantly, provide validation of several critical assumptions discussed in detail below.

6.4. Model Assumptions

[31] Two primary assumptions inherent in our detrital thermochronometry approach are that the catchments are uniformly sampled and that the sample sizes are adequate to describe the long-term erosion history of the source region.

6.4.1. Uniform Sampling Throughout the Catchment

[32] Differences in geomorphic processes (e.g., glacial, fluvial, or landsliding) and bedrock geology (e.g., variable concentrations in type and quality of target minerals) can lead to non-uniform sampling [*Brewer et al.*, 2006; *Stock et al.*, 2006; *Vermeesch*, 2007; *Avdeev et al.*, 2011; *Tranel et al.*, 2011] and, potentially, failure of a detrital sample to comprehensively represent the source region [*Amidon et al.*, 2005]. Ultimately, in detrital long-term erosion studies, the relevant questions are: to what degree is the uniform sampling assumption violated and how does it affect our data interpretation on a per catchment basis? In order to consider these questions, *Tranel et al.* [2011] suggest a paired bedrock and detrital approach for studies seeking to define the long-term erosion history of a catchment. Detailed characterization of bedrock cooling histories is not always feasible for broad-scale studies, as is the case in our eastern Tibet study where bedrock is poorly exposed and/or access within this vast and remote region is limited (Figure 1). Despite this limitation, we are able to validate our model assumptions through comparison of apatite fission track ages with helium ages as well as using model goodness-of-fit plots [*Avdeev et al.*, 2011].

[33] A focusing of erosion at low elevations, as might be expected in regions dominated by transient fluvial incision such as the eastern margin of the Tibetan Plateau, could lead to an abundance of ages from the young end of the spectrum, potentially mimicking the signal of acceleration in exhumation. Such a scenario would be particularly problematic in low-temperature thermochronometric studies that define component age frequency peaks from a detrital sample [e.g., *Brandon*, 2002] and interpret these as regional cooling events related to tectonic exhumation in the source region [e.g., *Willingshofer et al.*, 2001; *Coutand et al.*, 2006; *Carrapa and DeCelles*, 2008]. However, in the inversion method that we utilize here, the probability distributions of erosion rates through time, as well as depth to the partial retention zone, are resolved using the range of observed ages and uncertainties along with catchment hypsometry. Thus, the probability of the timing of a change in erosion rate is determined based on the entire spread in ages, not just the occurrence of young ages, and must result in reasonable closure isotherm elevations.

[34] Non-uniform spatial erosion rate, limited distributions of rocks that contain apatite, and a bias toward younger detrital ages or quality of apatite grains can be assessed from the goodness of fit plots and the comparison of helium to AFT data. Goodness of fit plots show a substantial mismatch between the observed and synthetic data for catchments modeled assuming a constant erosion rate (Figure 7) indicating that either our uniform sampling assumption is invalid or that the studied catchments have undergone a more complex (e.g., multistage) erosion history. The fact that the observed mismatch in the constant erosion case is mostly resolved by modeling detrital ages with a two-stage erosion

history that assumes uniform sampling (Figure 6) suggests that spatially non-uniform sampling influence is minor for our studied catchments. Moreover, the observed range in ages (Mesozoic through late Cenozoic), regardless of their probability distribution, cannot be explained simply by a constant erosion rate with non-uniform sampling, due to the fact that projecting a reasonable modern closure isotherm depth is not possible with this scenario.

[35] The similarly wide and well-distributed range in AHe and AFT ages, as well as variability in grain quality across study samples, also suggests that grains are broadly sourced from within the catchments and that basins are large enough to average out temporal and spatial point sources. Coherent exhumation histories derived from each chronometer independently also suggests that grain quality did not bias our age distributions because each technique has different analytical methods, limitations, and associated errors as well as grain size and quality requirements. Further, previous thermochronometry studies from the most common rocks in our study area demonstrate broad availability of apatite in our catchments [*Xu and Kamp*, 2000; *Wilson and Fowler*, 2011].

[36] Comparison of independent AHe and AFT modeling results do suggest that point-source biases may have a noticeable effect on the Yellow_small sample. Results show a different AHe age distribution and model result for the Yellow_small catchment in comparison to those of the adjacent, larger Yellow River catchment (Figure 6 and Table 2), yet fission track age distributions and associated model results are very similar for both catchments. One possible explanation for this discrepancy relates to biasing during apatite grain selection as a specific size and quality is required for helium analysis. Only two mapped geologic units comprise the smaller Yellow drainage basin: Jurassic granite of Mt. Lunag Dungze (between 4600 m and 5200 m elevation) and Triassic marine facies of the Songpan Ganzi complex (below 4600 m elevation). Although samples from the Songpan Ganzi deposits have yielded apatite, the concentration of heavy minerals is unlikely to be uniform throughout this ~10–20 km thick sequence of turbidite deposits [*Weislogel*, 2008]. Given this geologic pattern and the smaller catchment size of the Yellow_small drainage basin, it is possible that apatite suitable for helium dating is not well distributed throughout this catchment. Rather, the sample may be dominated by grains from granitoid rocks present at higher elevations, causing a disproportionate influx of older ages. Bedrock data would allow for further assessment of the validity or degree of such biasing.

6.4.2. Sample Size and Erosion Rate Estimations

[37] A wide range in AHe and AFT ages also supports our assumption that 20–40 grains, as analyzed here, are sufficient to characterize catchment age distributions. It has been suggested that dating ~100 grains per sample is required in detrital thermochronometry studies [*Hodges et al.*, 2005]; a rule of thumb stemming largely from work that determined the number of grains necessary for complete characterization of detrital mineral suites in provenance studies [*Vermeesch*, 2004]. Provenance studies require such high-density sampling in order to characterize discrete and unknown numbers of episodes of mineral crystallization. On the other hand, in general, low-temperature detrital cooling ages reflect the continuous cooling of rock as it is exhumed toward the surface of the Earth; therefore, exhumation ages should have a predictable relationship with elevation, which serves as a proxy for depth below the cooling surface. As a result, far fewer grains (as few as 5) may provide useful information in thermochronometry studies that incorporate basin hypsometry [*Avdeev et al.*, 2011]. Moreover, our approach does not always require a specific number of grains, but rather, the actual number will depend on the complexity of the exhumation model considered and the desired precision of estimated parameters in each particular study.

[38] Goodness-of-fit plots of model results from this study show that a constant erosion rate model can be rejected and reasonable exhumation parameters for the two-and three-stage erosion histories can be estimated from sample sizes of ~20 grains per catchment. Models with more than three stages of erosion do not produce significantly different erosion histories. Comparison of the Mekong and neighboring Mekong(b) catchment, which share similar erosion histories, further supports the reliability of our sample size. Due to low apatite yields, Mekong(b) has no fission track ages and 50% fewer AHe ages. Both Mekong(b) (AHe N=10) and Mekong (AHe N=20) are well fit by a two-stage erosion history with a late Cenozoic increase in erosion rate (see Figure S5), though the larger sample size for the Mekong does result in a higher precision estimate of the timing of erosion-rate increase (15–10 Ma as opposed to 20–1 Ma for Mekong(b)).

[39] Fast exhumation can result in heat advection that significantly alters the thermal field thereby invalidating the assumption of constant geothermal gradient in time and complicating interpretation of erosion rates from age/elevation relationships [*Moore and England*, 2001]. However, a geotherm approximated as constant is appropriate in this study because a combination of maximum possible erosion rates (<1 mm/yr) and cooling duration (<15 Myr) yields <20% increase in thermal gradient [*Ehlers*, 2005].

7. Discussion

[40] Erosion histories from the externally drained portion of the Tibetan Plateau potentially provide a record of surface uplift and climate conditions during orogen evolution, though erosion histories alone do not uniquely indicate a given tectonic or climatic scenario. Specifically, our samples should be sensitive to expansion of high topography related to plateau growth following continental collision because sample ages range from pre-collision through recent time. In addition, because the catchments we study are at or near the headwaters of major rivers that drain off the plateau, erosion histories are also potentially sensitive to upstream propagation of erosion signals that originate on the plateau perimeter. By comparing our results to studies on the same rivers at the plateau margins, we can evaluate whether or not the subdued topography of the interior of Tibet is isolated from erosion rates affecting its margins. Isolation from base-level changes by either slow or stalled knickpoint propagation [*Ouimet*, 2007; *Whipple*, 2010] has been suggested as a means by which the interior of Tibet has been or will continue to be protected from erosion allowing the plateau to remain high and relatively flat.

[41] Despite differences in precipitation, mean drainage-basin slope and relief, catchments spanning over 6° latitude share similar erosion histories (Figures 2 and 10). To first order, regional slow erosion for much of the Cenozoic must

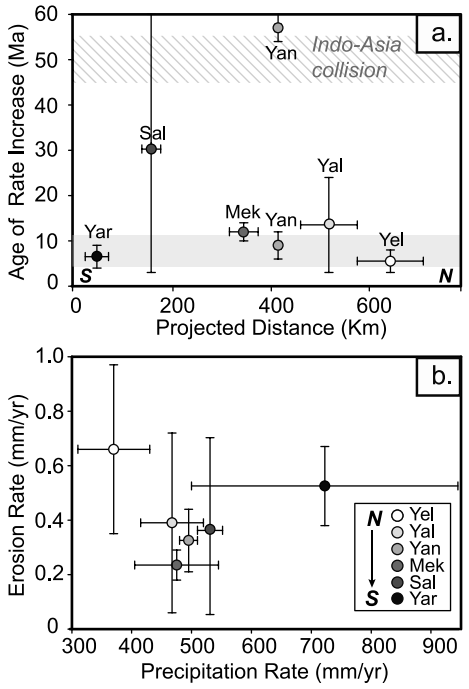

Figure 10. (a) Summary plot of the timing of late Cenozoic erosion rate increase within large catchments studied; Yar, Yarlung; Sal, Salween; Mek, Mekong; Yan, Yangtze; Yal, Yalong; Yel, Yellow. The *x* axis plots the catchments in order from south to north with distance away from the eastern syntaxis (black star in Figure 2b). Error bars reflect catchment width. The *y* axis shows the age of erosion rate increase (Ma). Error bars show the age range (within 95% confidence) in Ma for each catchment determined from preferred individual model results (Table 3). Gray swath shows age range (11–4 Ma) from the common erosion history model (Figure 9). Hatched gray swath shows the approximate timing of India-Asia continental collision. (b) Plot of mean annual precipitation rate (mm/yr) across each catchment (Matsuura and Willmott, online data, 2007) against late Cenozoic erosion rate (mm/yr) within 95% confidence (Table 3). Ranges in precipitation rate reflect the minimum and maximum cell values within each catchment (Figure 2b). Note the lack of obvious positive correlation between precipitation and erosion rates as is expected (see text for details).

be followed by a recent and widespread increase in erosion rate in order to preserve both old and young ages observed in each individual catchment. Inverse modeling results confirm that data are poorly fit by a constant erosion rate model and instead require increases in erosion rate since at least the mid-to-late Miocene in order to adequately describe the data (Figure 8). Posterior probabilities of the timing of increased erosion are centered during the mid-to-late Miocene for four of the studied catchments (Yarlung, Mekong, Yangtze, Yellow) indicating a regional pattern of increased erosion rate beginning over a 7 Myr period (Figure 10). Such an erosion history is also permissible by the other large catchments studied (Salween, Yalong), although the lack of ages younger than 13 Ma in these catchments do not allow precise constraints on the timing of rate change.

[42] Although the estimated timing of erosion rate change for the Yellow River catchment is consistent with the others, the high spread in AHe and AFT ages, as well as the presence of such a young age (4 Ma) within this sample, is somewhat surprising given the lower relief of this drainage basin (Table 2). Model results that show an increase to a higher erosion rate for this catchment, as compared to the others (Figure 8 and Table 3), can at least partially account for these differences in age and morphology. However, this catchment lies in an arid climate, thus we propose the rate is more sensitive to local faulting influence, possibly associated with the nearby Kunlun Fault (Figure 1). If true, the effect from local faulting appears to be only a subordinate component of the exhumation history of this catchment given the fairly smooth distribution of ages and the similarity of the age spread in the Yellow River as compared to the other catchments (Figure 6).

[43] Sample sites within the center of the study transect along eastward draining rivers appear to have an earlier onset of increased erosion rate (mid-to-late Miocene) as compared to sample sites on the northern and southern edges of the plateau (Miocene to early Pliocene) (Figure 10a). The 11–4 Ma age range found from a common-erosion history model for all of the catchments may encompass real variability in the timing of erosion rate change within 7 Myr or may be due to imperfect sampling of catchment surfaces. If the age variability is real, we imagine either a time-transgressive response of individual fluvial systems to common base-level change or uplift event, or true spatial variability in tectonic or climatic forcing across the plateau interior. Future work, including additional analyses from these samples and other smaller catchments along the study transect, may potentially highlight important nuances in the erosional response to forcing, geomorphic processes, and details in the spatial variability of the tectonic record.

[44] An earlier erosion event at 60–54 Ma is observed in the Yangtze catchment, though of lesser magnitude than the late Miocene event. Models that allow for two breaks in slope do not produce significantly better data fits for the other individual catchments. Yet, the simultaneous inversion of all data assuming a common erosion history shows that a widespread change in erosion rate at ~55 Ma is permissible, albeit the erosion rates still remain fairly low (<0.1 mm/yr).

7.1. Implications With Respect to Previous Tibetan Erosion Studies

[45] Extensive preservation of low-relief relict-landscape remnants [*Clark et al.*, 2006], knickpoints in river profiles, and variability in short-term erosion rates have been cited as evidence that late-Miocene incision of the eastern margin of the Tibetan Plateau has yet to equilibrate throughout the landscape [*Clark et al.*, 2006; *Ouimet et al.*, 2010]. *Ouimet et al.* [2010] also proposed that the erosion increase on the eastern plateau margin has not yet propagated into the headwaters of the major rivers. Similarity in timing between our results and accelerated erosion downstream suggests an incision signal may have in fact reached the headwaters of eastern Tibet along the trunk rivers. Elevation transects of apatite and zircon helium and apatite fission track collected over short horizontal distances in the Dadu, Yalong, and Yangtze River gorges [*Clark et al.*, 2005; *Ouimet et al.*, 2010], in the Longmen Shan [*Kirby et al.*, 2002; *Godard*

et al., 2009b], and from a regional study of the eastern plateau margin [*Wilson and Fowler*, 2011] (Figure 2a) record an onset of rapid fluvial incision into a regional low-relief surface across the eastern margin of the Tibetan Plateau between 15 and 5 Ma compared to between 11 and 4 Ma from the detrital data presented here. Bedrock data from elevation transects show a change in erosion rate from 0.01 to 0.06 to 0.25–5 mm/yr compared to catchment-wide increases in erosion rate from a slowly eroding landscape (∼0.005 mm/yr) to ∼0.2–0.6 mm/yr from this study. The similarity in timing between our results and accelerated erosion downstream suggests that the relatively low-relief interior of east-central Tibet is not protected from dissection by slow or stalled knickpoint migration along trunk rivers [*Ouimet et al.*, 2007; *Korup and Montgomery*, 2008]. Similar to reaches on the plateau perimeter, isolated relict surface remnants and early Cenozoic to Mesozoic helium ages in the headwater region suggest that the landscape is adjusting to new conditions [*Clark et al.*, 2005; *Ouimet et al.*, 2010]. Mesozoic (U-Th)/He cooling ages and fission track ages across eastern Tibet also preclude significant burial of the high-plateau surface as suggested by *Liu-Zeng et al.* [2008].

[46] Estimates of long-term erosion rates since late Miocene time from low-temperature thermochronology are consistent with short-term (10^2–10^5 yr) erosion rates measured with cosmogenic ^{10}Be within the Dadu, Yalong, and Yangtze gorges (∼0.3–0.5 mm/yr) [*Ouimet et al.*, 2009] as well as the headwaters of the Salween, Mekong, and Yalong rivers (∼0.1–0.2 mm/yr [*Henck et al.*, 2011, Figure 4]). However, millennial erosion rates vary locally from 0.01 to 8 mm/yr within the Three Rivers Region, an area of focused high rock-uplift rates [*Henck et al.*, 2011].

[47] The Yarlung River has a much more limited range of AHe and AFT ages (22–2 Ma) and significantly higher catchment relief (Figures 2 and 6), despite broadly similar timing and rates of increased erosion as compared to the other catchments. Higher erosion rates from the early Miocene to the late Miocene (∼0.1 mm/yr compared to ∼0.005 mm/yr; Figure 8) likely contribute to the difference in relief between this catchment and the others. Erosion events that account for 1–2 km of exhumation since 2 Ma (i.e., more recent than the youngest thermochronometric ages measured) cannot be resolved with our approach. Thus, it is possible that modern and/or Quaternary erosion rates are also higher within this catchment due to glaciation and/or the northward expansion of the eastern Himalayan syntaxis [*Seward and Burg*, 2008]. It is also noteworthy that we find erosion rates of ∼0.4 mm/yr within the Yarlung catchment (Figure 8). Thus, despite its proximity to the eastern Himalaya indenter corner, very rapid exhumation rates (3–5 mm/yr) [*Burg et al.*, 1997, 1998] are locally confined to within ∼60 km of Namche Barwa [*Seward and Burg*, 2008], and do not extend (yet) throughout the catchment, at least on geologic timescales.

[48] Rates of clastic sediment accumulation offshore of Southeast Asia have been used as proxies for rates of continental erosion [*Clift et al.*, 2002; *Clift*, 2006; *Clift and Sun*, 2006]. Recent sediment budgets derived from compilations of seismic data from Asian marginal seas show that sediment flux first peaked in the early middle Miocene, which is thought to relate to increases in precipitation and possibly rock-uplift rate [*Clift*, 2006]. Our results indicate slow erosion within east-central Tibet before the late Miocene. Thus, the pulse of sedimentation offshore is not likely correlative with an erosion event in the headwaters of the Tibetan Plateau at this time.

7.2. Impact of Climate on Tibetan Plateau Erosion Rates

[49] Our results show no obvious correlation between erosion and precipitation rates across the study site or when comparing the high plateau to the wetter eastern plateau margin. Modern mean annual precipitation amounts increase across the study transect from south to north (∼600 mm/yr in the south to ∼300 mm/yr in the north [*New et al.*, 2002]). Isotopic evidence supports that the northern plateau was arid by Neogene time [*Dettman et al.*, 2003; *Kent-Corson et al.*, 2009], which suggests that modern trends in precipitation existed in the geologic past. A correlated pattern of northward-decreasing erosion rates is not borne out in our results (Figure 10b). Instead, the catchments with the highest erosion rates (Yarlung and Yellow) are in the wettest and driest regions, respectively (Figure 2 and Table 3). These catchments are also characterized by extremes in mean catchment relief and slope (Figure 2). Moreover, erosion rates from our sites on the Tibetan Plateau highland are very similar to rates from the high-precipitation eastern plateau margin (>1000 mm/yr mean annual precipitation [*New et al.*, 2002]).

[50] The shift to increased erosion rates between 11 and 4 Ma overlaps broadly with the timing of various purported climate changes in Asia at about 10 Ma, many of which have been linked with strengthening monsoon intensity (see review by *Molnar et al.* [2010], and references therein). However, correlating climatic events with changes in erosion rates is difficult in the east-central Tibetan Plateau. Although in some cases increased precipitation has been shown to drive enhanced erosion [e.g., *Brozović et al.*, 1997; *Montgomery et al.*, 2001; *Reiners et al.*, 2003; *Thiede et al.*, 2004], our results are consistent with other studies that suggest that there is not always a direct influence of precipitation on erosion rates [e.g., *Riebe et al.*, 2001; *Burbank et al.*, 2003; *Finnegan et al.*, 2008; *Binnie et al.*, 2010; *Henck et al.*, 2011]. Relating erosion rate changes to climatic events is further complicated by complex moisture source interactions in this region [e.g., *Hren et al.*, 2009], particularly with respect to the monsoonal systems. The Asian monsoon systems surely influence study catchments but not necessarily to the same degree across the sampling transect. Furthermore, a lack of understanding as to how the monsoonal systems along the eastern plateau have evolved through time yields even greater uncertainty in speculating the role of climate change on erosion history in this region.

[51] Although erosion histories alone cannot be used to definitively discern the relative roles of climatic and tectonic processes, it is unlikely that monsoon strengthening is the sole driver of the observed increase in erosion rates at 11–4 Ma. Attributing erosion-rate increases exclusively to climatic changes requires that high topography existed in the east-central plateau prior to at least the middle Miocene. Significant pre-collision crustal shortening and thickening are suggested within the southern central Tibetan Plateau [*Murphy et al.*, 1997; *Kapp et al.*, 2005, 2007; *DeCelles et al.*, 2007] and paleoaltimetry studies support that high

elevations existed within this region by early Miocene time [*Garzione et al.*, 2000; *Rowley et al.*, 2001; *Spicer et al.*, 2003; *Currie et al.*, 2005; *Cyr et al.*, 2005; *Rowley and Currie*, 2006; *DeCelles et al.*, 2007; *Polissar et al.*, 2009]. Along the eastern plateau, our results show constant low erosion rates throughout the early and middle Cenozoic. Thus, creation of this high topography prior to 11–4 Ma would have occurred without discernable widespread increases in erosion rate, which seems improbable. If the rivers of this region were internally drained in the past, surface uplift could occur without discernable increases in erosion rate. However, there is no evidence in the large-scale drainage patterns to suggest major reorganization from isolated paleo-basins to the current externally drained system [*Clark et al.*, 2004]. Perhaps a more likely scenario is that the creation of high topography, changes in climate, and increased erosion rates are linked such that both surface uplift and an associated stronger monsoon system acted in concert to drive higher erosion rates across east-central Tibet.

7.3. Tectonic Interpretation of Tibetan Plateau Erosion Patterns

[52] A common prediction of many tectonic scenarios for Tibet is the northward propagation of topography since collision time. If the onset of increased erosion rates across the east-central Tibetan Plateau interior is interpreted as a proxy for the timing of significant elevation increase, the spatial patterns in erosion documented here challenge competing descriptions of plateau development. Mechanical and geodynamic models of Tibetan Plateau formation as disparate as localized shear and stepwise growth [e.g., *Tapponnier et al.*, 2001], distributed shortening and thickening of Asian lithosphere [e.g., *England and Houseman*, 1986], and underthrusting of Indian crust and/or lithosphere [e.g., *Powell*, 1986] share the common prediction of topographic growth progressing northward away from the collision boundary with time. If Tibet grew by appending material to a northward-expanding deformation front starting with initial collision circa 50 Ma, then we expect a similarly migrating front of high erosion rates either continuously or in stages. Results from this study, which document relatively uniform rather than spatial or temporal progressions in timing or rates of erosion, are inconsistent with this prediction across the east-central high plateau. The resolution of our results do permit the possibility of spatial patterns in erosion over an ~7 million year time window during the mid-to-late Miocene to early Pliocene. However, this time frame of propagation would occur well after collision and over a shorter time duration than predicted for these sequential tectonic models.

[53] Nor do our results support the proposition of widespread surface uplift of the eastern plateau at 40 Ma [*Chung et al.*, 1998] or that an early Cenozoic central nucleus of high topography grew outward to the south and north as collision progressed [*Wang et al.*, 2008]. An Eocene increase in erosion rate within the Yangtze and possibly the other catchments, is roughly coincident with the timing of Indo-Asian collision [*Rowley*, 1996, 1998]. Fault studies in the Yushu-Nangqian region in close proximity to the Yangtze catchment, suggest contractional deformation from prior to 50 Ma to 37 Ma [*Spurlin et al.*, 2005]. Eocene faulting thought to be related to collision has also been identified across the northern margin of Tibet [*Yin et al.*, 2008; *Clark et al.*, 2010; *Duvall et al.*, 2011; *Clark*, 2012] and in the Fenghuo Shan-Nangqian thrust belt in central Tibet [*Horton et al.*, 2002; *Liu et al.*, 2003; *Wang et al.*, 2008]. A subtle Eocene increase in erosion rate could signify widespread faulting close to collision time, but we suggest that it was not accompanied by regional surface uplift that affected the eastern plateau.

[54] We find that the timing of increased erosion rate is similar across the length of our sampling transect. Thus, our results are generally consistent with processes thought to result in wide-spread, uniform surface uplift such as loss of a mantle root [*Molnar et al.*, 1993], injection of Indian crust into Tibetan lower crust [*Zhao and Morgan*, 1987], or channel flow [*Bird*, 1991; *Royden*, 1996; *Clark and Royden*, 2000; *Royden et al.*, 2008]. Late Miocene initiation of major river incision within the easternmost margin of Tibet (Figure 2) [*Clark et al.*, 2005; *Ouimet et al.*, 2010; *Wilson and Fowler*, 2011] has been proposed to relate to broad long-wavelength uplift due to crustal thickening by lower crustal flow [*Clark and Royden*, 2000; *Kirby et al.*, 2002; *Clark et al.*, 2006; *Royden et al.*, 2008; *Ouimet et al.*, 2010]. A late-Miocene shift to increased erosion rate is also observed along our study transect (Figure 10a) and the magnitude of erosion rates after this shift is similar in each region, suggesting the possibility that surface uplift, possibly related to lower crustal flow, may have influenced this entire eastern plateau region. Due to the relatively broad range in estimated timing of onset of increased erosion rates in both locations (15–5 Ma in the eastern margin of the Tibetan Plateau and 11–4 Ma from this study), we cannot conclude if increased erosion rates occurred truly simultaneously or if rates increased first in the east and then later in the west as knickpoints moved upstream or if a rate increase propagated from west to east relating to a migrating front of lower-crustal material. Testing specific predictions of west-to-east (or vice versa) propagation within a 10 million year window requires more precise estimates in timing.

8. Conclusions

[55] This study determines patterns in erosion rates and timing of erosion-rate change across the east-central Tibetan Plateau interior by measurements of low-temperature thermochronometry in detrital apatites collected from modern river sands. The following points summarize the main conclusions from this work, which have implications regarding Tibetan Plateau tectonic and geomorphic evolution.

[56] 1. AHe and AFT ages range widely within all but one of the large catchments studied, which suggests that erosion histories are relatively uniform among catchments that span the entire width of the east-central Tibetan Plateau. Generalized modeling results show a long period of slow (~0.005 mm/yr) or no erosion until the late Cenozoic (11–4 Ma) when an abrupt increase to faster erosion rates (~0.2–0.6 mm/yr) occurred. The timing and rates of increased erosion found in this study also overlap results from the eastern plateau margin.

[57] 2. Uniform, slow erosion across the eastern width of Tibet until the late Cenozoic does not support a steep propagating plateau migrating to the north from collision time,

as is predicted for many geodynamic and mechanical descriptions of plateau evolution.

[58] 3. Although we cannot definitively distinguish between tectonic and climatic influences on the erosion record from this data set alone, our results are consistent with broad surface uplift as the main driver of late Cenozoic erosion rate increase. We suggest that regional uplift potentially relates to flux of lower crustal material into this region, driving widespread and abrupt increases in erosion rate across the east-central Tibetan Plateau. We also relate a smaller-magnitude Eocene erosional event to local surface faulting associated with Indo-Asian plate collision.

[59] 4. We find no obvious correlation between erosion rate and precipitation either across the study site or when comparing to erosion rates within much wetter parts of the plateau (i.e., the eastern plateau perimeter). Erosion rates and timing of rate increases are commensurate along upstream and downstream sections of the major rivers draining Tibet. Thus, fluvial reaches within the Tibetan highlands are not isolated from base-level changes by a migrating knickpoint that has yet to drive into the headwaters regions, as has been thought previously.

[60] **Acknowledgments.** Boris Avdeev passed away unexpectedly during the final copyediting stages of this manuscript. We recognize his full input to what is published here and wish to dedicate the paper to his memory. His intellectual creativity and adventurous spirit will always inspire us. This work was supported by the NSF grants EAR-0507431, EAR-0908711, EAR-0507788, and EAR-0810067; the National Science Foundation of China (40234040; and the State Key Laboratory of Earthquake Dynamics (LED2008A01). We thank Lindsay Hedges and William Amidon for assistance with sample analyses, John Bershaw and Pei-zhen Zhang for field support, and Nora Lewandowski and Joe Murphy for help with mineral separations. We thank Jim Spotila and Barbara Carrapa for thoughtful and constructive reviews. We also acknowledge Doug Burbank, Nathan Niemi, Eric Kirby, and Peter Molnar for thoughtful discussions about this work.

References

Amidon, W. H., D. W. Burbank, and G. E. Gehrels (2005), Construction of detrital mineral populations: Insights from the mixing of U-Pb zircon ages in Himalayan rivers, *Basin Res.*, *17*(4), 463–485, doi:10.1111/j.1365-2117.2005.00279.x.

An, Z., J. E. Kutzbach, W. L. Prell, and S. C. Porter (2001), Evolution of Asian monsoons and phased uplift of the Himalaya–Tibetan plateau since Late Miocene times, *Nature*, *411*(6833), 62–66, doi:10.1038/35075035.

Argand, E. (1924), La tectonique de l'Asie, *Proc. Int. Geol. Congr.*, *13*, 171–372.

Arne, D., B. Worley, C. Wilson, S. F. Chen, D. Foster, Z. L. Luo, S. G. Liu, and P. Dirks (1997), Differential exhumation in response to episodic thrusting along the eastern margin of the Tibetan Plateau, *Tectonophysics*, *280*(3–4), 239–256, doi:10.1016/S0040-1951(97)00040-1.

Avdeev, B., N. A. Niemi, and M. K. Clark (2011), Doing more with less: Bayesian estimation of erosion models with detrital thermochronometric data, *Earth Planet. Sci. Lett.*, *305*, 385–395, doi:10.1016/j.epsl.2011.03.020.

Binnie, S. A., W. M. Phillips, M. A. Summerfield, L. K. Fifield, and J. A. Spotila (2010), Tectonic and climatic controls of denudation rates in active orogens: The San Bernardino Mountains, California, *Geomorphology*, *118*, 249–261, doi:10.1016/j.geomorph.2010.01.005.

Bird, P. (1991), Lateral extrusion of lower crust from under high topography in the isostatic limit, *J. Geophys. Res.*, *96*, 10,275–10,286, doi:10.1029/91JB00370.

Boos, W. R., and Z. M. Kuang (2010), Dominant control of the South Asian monsoon by orographic insulation versus plateau heating, *Nature*, *463*, 218–222, doi:10.1038/nature08707.

Booth, A. L., P. K. Zeitler, W. S. F. Kidd, J. Wooden, Y. Liu, B. Idleman, M. Hren, and C. P. Chamberlain (2004), U-Pb zircon constraints on the tectonic evolution of southeastern Tibet, Namche Barwa Area, *Am. J. Sci.*, *304*, 889–929, doi:10.2475/ajs.304.10.889.

Booth, A. L., C. P. Chamberlain, W. S. F. Kidd, and P. K. Zeitler (2009), Constraints on the metamorphic evolution of the eastern Himalayan syntaxis from geochronologic and petrologic studies of Namche Barwa, *Geol. Soc. Am. Bull.*, *121*, 385–407, doi:10.1130/B26041.1.

Brandon, M. T. (2002), Decomposition of mixed grain age distributions using BINOMFIT, *On Track*, *12*(24), 1–18.

Braun, J. (2002), Quantifying the effect of recent relief changes on age-elevation relationships, *Earth Planet. Sci. Lett.*, *200*, 331–343, doi:10.1016/S0012-821X(02)00638-6.

Brewer, I. D., D. W. Burbank, and K. V. Hodges (2003), Modelling detrital cooling-age populations: Insights from two Himalayan catchments, *Basin Res.*, *15*, 305–320, doi:10.1046/j.1365-2117.2003.00211.x.

Brewer, I. D., D. W. Burbank, and K. V. Hodges (2006), Downstream development of a detrital cooling-age signal: Insights from $^{40}Ar/^{39}Ar$ muscovite thermochronology in the Nepalese Himalaya, in *Tectonics, Climate, and Landscape Evolution*, edited by S. D. Willett et al., *Spec. Pap. Geol. Soc. Am.*, *398*, 321–338, doi:10.1130/2006.2398(20).

Brozović, N., D. W. Burbank, and A. J. Meigs (1997), Climatic limits on landscape development in the northwestern Himalaya, *Science*, *276*, 571–574, doi:10.1126/science.276.5312.571.

Burbank, D. W., A. E. Blythe, J. Putkonen, B. Pratt-Sitaula, E. Gabet, M. Oskin, A. Barros, and T. P. Ojha (2003), Decoupling of erosion and precipitation in the Himalayas, *Nature*, *426*, 652–655, doi:10.1038/nature02187.

Burg, J. P., P. Davy, P. Nievergelt, F. Oberli, D. Seward, Z. Z. Diao, and M. Meier (1997), Exhumation during crustal folding in the Namche-Barwa syntaxis, *Terra Nova*, *9*, 53–56, doi:10.1111/j.1365-3121.1997.tb00001.x.

Burg, J. P., P. Nievergelt, F. Oberli, D. Seward, P. Davy, J. C. Maurin, Z. Z. Diao, and M. Meier (1998), The Namche Barwa syntaxis: Evidence for exhumation related to compressional crustal folding, *J. Asian Earth Sci.*, *16*, 239–252, doi:10.1016/S0743-9547(98)00002-6.

Carrapa, B., and P. G. DeCelles (2008), Eocene exhumation and basin development in the Puna of northwestern Argentina, *Tectonics*, *27*, TC1015, doi:10.1029/2007TC002127.

Chen, W.-P., S.-H. Hung, T.-L. Tseng, M. Brudzinski, Z. Yang, and R. L. Nowack (2012), Rheology of the continental lithosphere: Progress and new perspectives, *Gondwana Res.*, *21*, 4–18, doi:10.1016/j.gr.2011.07.013.

Chung, S. L., C. H. Lo, T. Y. Lee, Y. Q. Zhang, Y. W. Xie, X. H. Li, K. L. Wang, and P. L. Wang (1998), Diachronous uplift of the Tibetan plateau starting 40 Myr ago, *Nature*, *394*, 769–773, doi:10.1038/29511.

Clark, M. K. (2012), Slowing of continental collision due to viscous mantle lithosphere rather than topography, *Nature*, *483*, 74–77, doi:10.1038/nature10848.

Clark, M. K., and L. H. Royden (2000), Topographic ooze: Building the eastern margin of Tibet by lower crustal flow, *Geology*, *28*, 703–706, doi:10.1130/0091-7613(2000)28<703:TOBTEM>2.0.CO;2.

Clark, M. K., L. M. Schoenbohm, L. H. Royden, K. X. Whipple, B. C. Burchfiel, X. Zhang, W. Tang, E. Wang, and L. Chen (2004), Surface uplift, tectonics, and erosion of eastern Tibet from large-scale drainage patterns, *Tectonics*, *23*, TC1006, doi:10.1029/2002TC001402.

Clark, M. K., M. A. House, L. H. Royden, K. X. Whipple, B. C. Burchfiel, X. Zhang, and W. Tang (2005), Late Cenozoic uplift of southeastern Tibet, *Geology*, *33*, 525–528, doi:10.1130/G21265.1.

Clark, M. K., L. H. Royden, K. X. Whipple, B. C. Burchfiel, X. Zhang, and W. Tang (2006), Use of a regional, relict landscape to measure vertical deformation of the eastern Tibetan Plateau, *J. Geophys. Res.*, *111*, F03002, doi:10.1029/2005JF000294.

Clark, M. K., K. A. Farley, D. W. Zheng, Z. C. Wang, and A. R. Duvall (2010), Early Cenozoic faulting of the northern Tibetan Plateau margin from apatite (U-Th)/He ages, *Earth Planet. Sci. Lett.*, *296*, 78–88, doi:10.1016/j.epsl.2010.04.051.

Clift, P. D. (2006), Controls on the erosion of Cenozoic Asia and the flux of clastic sediment to the ocean, *Earth Planet. Sci. Lett.*, *241*, 571–580, doi:10.1016/j.epsl.2005.11.028.

Clift, P. D., and Z. Sun (2006), The sedimentary and tectonic evolution of the Yinggehai-Song Hong basin and the southern Hainan margin, South China Sea: Implications for Tibetan uplift and monsoon intensification, *J. Geophys. Res.*, *111*, B06405, doi:10.1029/2005JB004048.

Clift, P., J. Il Lee, M. K. Clark, and J. Blusztajn (2002), Erosional response of South China to arc rifting and monsoonal strengthening; a record from the South China Sea, *Mar. Geol.*, *184*, 207–226, doi:10.1016/S0025-3227(01)00301-2.

Cook, K. L., and L. H. Royden (2008), The role of crustal strength variations in shaping orogenic plateaus, with application to Tibet, *J. Geophys. Res.*, *113*, B08407, doi:10.1029/2007JB005457.

Coutand, I., B. Carrapa, A. Deeken, A. K. Schmitt, E. R. Sobel, and M. R. Strecker (2006), Propagation of orographic barriers along an active range front: Insights from sandstone petrography and detrital apatite fission-track thermochronology in the intermontane Angastaco

basin, NW Argentina, *Basin Res.*, *18*, 1–26, doi:10.1111/j.1365-2117.2006.00283.x.

Currie, B. S., D. B. Rowley, and N. J. Tabor (2005), Middle Miocene paleoaltimetry of southern Tibet: Implications for the role of mantle thickening and delamination in the Himalayan orogen, *Geology*, *33*, 181–184, doi:10.1130/G21170.1.

Cyr, A. J., B. S. Currie, and D. B. Rowley (2005), Geochemical evaluation of Fenghuoshan Group lacustrine carbonates, North-Central Tibet: Implications for the paleoaltimetry of the Eocene Tibetan Plateau, *J. Geol.*, *113*, 517–533, doi:10.1086/431907.

DeCelles, P. G., D. M. Robinson, and G. Zandt (2002), Implications of shortening in the Himalaya fold-thrust belt for uplift of the Tibetan Plateau, *Tectonics*, *21*(6), 1062, doi:10.1029/2001TC001322.

DeCelles, P. G., J. Quade, P. Kapp, M. J. Fan, D. L. Dettman, and L. Ding (2007), High and dry in central Tibet during the Late Oligocene, *Earth Planet. Sci. Lett.*, *253*, 389–401, doi:10.1016/j.epsl.2006.11.001.

DeGraaff-Surpless, K., J. B. Mahoney, J. L. Wooden, and M. O. McWilliams (2003), Lithofacies control in detrital zircon provenance studies: Insights from the Cretaceous Methow basin, southern Canadian Cordillera, *Geol. Soc. Am. Bull.*, *115*, 899–915, doi:10.1130/B25267.1.

Dettman, D. L., X. Fang, C. N. Garzone, and J. Li (2003), Uplift-drive climate change at 12 Ma: A long δ^{18}O record from the NE margin of the Tibetan Plateau, *Earth Planet. Sci. Lett.*, *214*, 267–277, doi:10.1016/S0012-821X(03)00383-2.

Dewey, J. F., R. M. Shackleton, C. Chengfa, and S. Yiyin (1988), The tectonic evolution of the Tibetan Plateau, *Philos. Trans. R. Soc. London A*, *327*, 379–413, doi:10.1098/rsta.1988.0135.

Ding, L., D. Zhong, A. Yin, P. Kapp, and T. M. Harrison (2001), Cenozoic structural and metamorphic evolution of the eastern Himalayan syntaxis (Namche Barwa), *Earth Planet. Sci. Lett.*, *192*, 423–438, doi:10.1016/S0012-821X(01)00463-0.

Dodson, M. (1973), Closure temperature in cooling geochronological and petrological systems, *Contrib. Mineral. Petrol.*, *40*, 259–274, doi:10.1007/BF00373790.

Donelick, R. A., P. B. O'Sullivan, and R. A. Ketcham (2005), Apatite fission-track analysis, in *Low-Temperature Thermochronology: Techniques, Interpretations, and Applications*, *Rev. Mineral. Geochem.*, vol. 58, edited by P. W. Reiners and T. A. Ehlers, pp. 49–94, Mineral. Soc. of Am., Washington, D. C.

Duvall, A. R., M. K. Clark, B. A. van der Pluijm, and C. Li (2011), Direct dating of Eocene reverse faulting in northeastern Tibet using Ar-dating of fault clays and low-temperature thermochronometry, *Earth Planet. Sci. Lett.*, *304*, 520–526, doi:10.1016/j.epsl.2011.02.028.

Ehlers, T. A. (2005), Crustal thermal processes and the interpretation of thermchronometer data, in *Low-Temperature Thermochronology: Techniques, Interpretations, and Applications*, *Rev. Mineral. Geochem.*, vol. 58, edited by P. W. Reiners and T. A. Ehlers, pp. 315–350, Mineral. Soc. of Am., Washington, D. C.

Ehlers, T. A., and K. A. Farley (2003), Apatite (U-Th)/He thermochronometry: Methods and applications to problems in tectonic and surface processes, *Earth Planet. Sci. Lett.*, *206*, 1–14, doi:10.1016/S0012-821X(02)01069-5.

England, P., and G. Houseman (1986), Finite strain calculations of continental deformation: 2. Comparison with the India-Asia Collision Zone, *J. Geophys. Res.*, *91*, 3664–3676, doi:10.1029/JB091iB03p03664.

England, P., and G. Houseman (1989), Extension during continental convergence, with application to the Tibetan Plateau, *J. Geophys. Res.*, *94*, 17,561–17,579, doi:10.1029/JB094iB12p17561.

England, P., and D. McKenzie (1982), A thin viscous sheet model for continental deformation, *Geophys. J. Int.*, *70*, 295–321, doi:10.1111/j.1365-246X.1982.tb04969.x.

Enkelmann, E., L. Ratschbacher, R. Jonckheere, R. Nestler, M. Fleischer, R. Gloaguen, B. R. Hacker, Y. Q. Zhang, and Y. S. Ma (2006), Cenozoic exhumation and deformation of northeastern Tibet and the Qinling: Is Tibetan lower crustal flow diverging around the Sichuan Basin?, *Geol. Soc. Am. Bull.*, *118*, 651–671, doi:10.1130/B25805.1.

Enkelmann, E., T. A. Ehlers, P. K. Zeitler, and B. Hallet (2011), Denudation of the Namche Barwa antiform, eastern Himalaya, *Earth Planet. Sci. Lett.*, *307*, 323–333, doi:10.1016/j.epsl.2011.05.004.

Farley, K. (2000), Helium diffusion from apatite: General behavior as illustrated by Durango fluorapatite, *J. Geophys. Res.*, *105*, 2903–2914, doi:10.1029/1999JB900348.

Farley, K. A., R. A. Wolf, and L. T. Silver (1996), The effects of long alpha-stopping distances on (U-Th)/He ages, *Geochim. Cosmochim. Acta*, *60*, 4223–4229, doi:10.1016/S0016-7037(96)00193-7.

Finnegan, N. J., B. Hallet, D. R. Montgomery, P. K. Zeitler, J. O. Stone, A. M. Anders, and L. Yuping (2008), Coupling of rock uplift and river incision in the Namche Barwa-Gyala Peri massif, Tibet, *Geol. Soc. Am. Bull.*, *120*, 142–155, doi:10.1130/B26224.1.

Fitzgerald, P. G., and A. J. W. Gleadow (1990), New approaches in fission-track geochronology as a tectonic tool: Examples from the transantarctic mountains, *Nucl. Tracks Radiat. Meas.*, *17*, 351–357, doi:10.1016/1359-0189(90)90057-5.

Flohn, H., M. Hantel, and E. Ruprecht (1968), Air-mass dynamics or subsidence processes in Arabian Sea summer monsoon, *J. Atmos. Sci.*, *25*, 527–529, doi:10.1175/1520-0469(1968)025<0527:AMDOSP>2.0.CO;2.

Flowers, R. M., D. L. Shuster, B. P. Wernicke, and K. A. Farley (2007), Radiation damage control on apatite (U-Th)/He dates from the Grand Canyon region, Colorado Plateau, *Geology*, *35*, 447–450, doi:10.1130/G23471A.1.

Flowers, R. M., R. A. Ketcham, D. L. Shuster, and K. A. Farley (2009), Apatite (U-Th)/He thermochronometry using a radiation damage accumulation and annealing model, *Geochim. Cosmochim. Acta*, *73*(8), 2347–2365, doi:10.1016/j.gca.2009.01.015.

Galbraith, R. (2005), *Statistics for Fission Track Analysis*, 219 pp., Chapman and Hall, Boca Raton, Fla., doi:10.1201/9781420034929.

Garzione, C. N., J. Quade, P. G. DeCelles, and N. B. English (2000), Predicting paleoelevation of Tibet and the Himalaya from delta O-18 vs. altitude gradients in meteoric water across the Nepal Himalaya, *Earth Planet. Sci. Lett.*, *183*, 215–229, doi:10.1016/S0012-821X(00)00252-1.

Gleadow, A., and I. Duddy (1981), A natural long-term track annealing experiment for apatite, *Nucl. Tracks*, *5*, 169–174, doi:10.1016/0191-278X(81)90039-1.

Godard, V., R. Cattin, and J. Lave (2009a), Erosional control on the dynamics of low-convergence rate continental plateau margins, *Geophys. J. Int.*, *179*, 763–777, doi:10.1111/j.1365-246X.2009.04324.x.

Godard, V., R. Pik, J. Lave, R. Cattin, B. Tibari, J. de Sigoyer, M. Pubellier, and J. Zhu (2009b), Late Cenozoic evolution of the central Longmen Shan, eastern Tibet: Insight from (U-Th)/He thermochronometry, *Tectonics*, *28*, TC5009, doi:10.1029/2008TC002407.

Henck, A. C., K. W. Huntington, J. O. Stone, D. R. Montgomery, and B. Hallet (2011), Spatial controls on erosion in the Three Rivers Region, southeastern Tibet and southwestern China, *Earth Planet. Sci. Lett.*, *303*, 71–83, doi:10.1016/j.epsl.2010.12.038.

Henderson, A. L., G. L. Foster, and Y. Najman (2010), Testing the application of in situ Sm-Nd isotopic analysis on detrital apatites: A provenance tool for constraining the timing of India-Eurasia collision, *Earth Planet. Sci. Lett.*, *297*, 42–49, doi:10.1016/j.epsl.2010.06.001.

Hodges, K., K. Ruhl, C. Wobus, and M. Pringle (2005), ^{40}Ar/^{39}Ar thermochronology of detrital minerals, in *Low-Temperature Thermochronology: Techniques, Interpretations, and Applications*, *Rev. Mineral. Geochem.*, vol. 58, edited by P. W. Reiners and T. A. Ehlers, pp. 239–257, Mineral. Soc. of Am., Washington, D. C.

Horton, B. K., A. Yin, M. S. Spurlin, J. Zhou, and J. Wang (2002), Paleocene–Eocene syncontractional sedimentation in narrow, lacustrine-dominated basins of east-central Tibet, *Geol. Soc. Am. Bull.*, *114*, 771–786, doi:10.1130/0016-7606(2002)114<0771:PESSIN>2.0.CO;2.

Hren, M. T., B. Bookhagen, P. M. Blisniuk, A. L. Booth, and C. P. Chamberlain (2009), δ^{18}O and δD of streamwaters across the Himalaya and Tibetan Plateau: Implications for moisture sources and paleoelevation reconstructions, *Earth Planet. Sci. Lett.*, *288*, 20–32, doi:10.1016/j.epsl.2009.08.041.

Hu, S., L. He, and J. Wang (2000), Heat flow in the continental area of China: A new data set, *Earth Planet. Sci. Lett.*, *179*, 407–419, doi:10.1016/S0012-821X(00)00126-6.

Jolivet, M., M. Brunel, D. Seward, Z. Xu, J. Yang, F. Roger, P. Tapponnier, J. Malavieille, N. Arnaud, and C. Wu (2001), Mesozoic and Cenozoic tectonics of the northern edge of the Tibetan plateau: Fission-track constraints, *Tectonophysics*, *343*, 111–134, doi:10.1016/S0040-1951(01)00196-2.

Kapp, P., A. Yin, T. M. Harrison, and L. Ding (2005), Cretaceous-Tertiary shortening, basin development, and volcanism in central Tibet, *Geol. Soc. Am. Bull.*, *117*, 865–878, doi:10.1130/B25595.1.

Kapp, P., P. G. DeCelles, G. E. Gehrels, M. Heizler, and L. Ding (2007), Geological records of the Lhasa-Qiangtang and Indo-Asia collisions in the Nima area of central Tibet, *Geol. Soc. Am. Bull.*, *119*, 917–933, doi:10.1130/B26033.1.

Kent-Corson, M. L., B. D. Ritts, G. Zhuang, P. M. Bovet, S. A. Graham, and C. P. Chamberlain (2009), Stable isotope constraints on the tectonic, topographic, and climate evolution of the northern margin of the Tibetan Plateau, *Earth Planet. Sci. Lett.*, *282*, 158–166, doi:10.1016/j.epsl.2009.03.011.

Ketcham, R. A., A. Carter, R. A. Donelick, J. Barbarand, and A. J. Hurford (2007), Improved modeling of fission-track annealing in apatite, *Am. Mineral.*, *92*, 799–810, doi:10.2138/am.2007.2281.

Kirby, E., P. W. Reiners, M. A. Krol, K. X. Whipple, K. V. Hodges, K. A. Farley, W. Q. Tang, and Z. L. Chen (2002), Late Cenozoic evolution of the eastern margin of the Tibetan Plateau: Inferences from

$^{40}Ar/^{39}Ar$ and (U-Th)/He thermochronology, *Tectonics*, *21*(1), 1001, doi:10.1029/2000TC001246.

Korup, O., and D. Montgomery (2008), Tibetan plateau river incision inhibited by glacial stabilization of the Tsangpo gorge, *Nature*, *455*, 786–789, doi:10.1038/nature07322.

Lal, D., N. B. W. Harris, K. K. Sharma, Z. Gu, L. Ding, T. Liu, W. Dong, M. W. Caffee, and A. Jull (2004), Erosion history of the Tibetan Plateau since the last interglacial: Constraints from the first studies of cosmogenic 10Be from Tibetan bedrock, *Earth Planet. Sci. Lett.*, *217*, 33–42, doi:10.1016/S0012-821X(03)00600-9.

Lease, R. O., D. W. Burbank, G. E. Gehrels, Z. C. Wang, and D. Y. Yuan (2007), Signatures of mountain building: Detrital zircon U/Pb ages from northeastern Tibet, *Geology*, *35*, 239–242, doi:10.1130/G23057A.1.

Lease, R. O., D. W. Burbank, M. K. Clark, K. A. Farley, D. Zheng, and H. Zhang (2011), Middle Miocene reorganization of deformation along the northeastern Tibetan Plateau, *Geology*, *39*, 359–362, doi:10.1130/G31356.1.

Li, C. F., and M. Yanai (1996), The onset and interannual variability of the Asian summer monsoon in relation to land sea thermal contrast, *J. Clim.*, *9*, 358–375, doi:10.1175/1520-0442(1996)009<0358:TOAIVO>2.0.CO;2.

Liu, Z., X. Zhao, C. Wang, S. Liu, and H. Yi (2003), Magnetostratigraphy of Tertiary sediments from the Hoh Xil Basin: Implications for the Cenozoic tectonic history of the Tibetan Plateau, *Geophys. J. Int.*, *154*, 233–252, doi:10.1046/j.1365-246X.2003.01986.x.

Liu-Zeng, J., P. Tapponnier, Y. Gaudemer, and L. Ding (2008), Quantifying landscape differences across the Tibetan plateau: Implications for topographic relief evolution, *J. Geophys. Res.*, *113*, F04018, doi:10.1029/2007JF000897.

Malloy, M. (2004), Rapid erosion at the Tsangpo knickpoint and exhumation of southeastern Tibet, MS thesis, 84 pp., Lehigh Univ., Bethlehem, Pa.

Mancktelow, N. S., and B. Grasemann (1997), Time-dependent effects of heat advection and topography on cooling histories during erosion, *Tectonophysics*, *270*, 167–195, doi:10.1016/S0040-1951(96)00279-X.

Molnar, P. (2005), Mio-pliocene growth of the Tibetan Plateau and evolution of East Asian climate, *Palaeontol. Electron.*, *8*(1), 8.1.2A.

Molnar, P., P. England, and J. Martinod (1993), Mantle dynamics, uplift of the Tibetan Plateau, and the Indian Monsoon, *Rev. Geophys.*, *31*, 357–396, doi:10.1029/93RG02030.

Molnar, P., W. R. Boos, and D. S. Battisti (2010), Orographic controls on climate and paleoclimate of Asia: Thermal and mechanical roles for the Tibetan Plateau, *Annu. Rev. Earth Planet. Sci.*, *38*, 77–102, doi:10.1146/annurev-earth-040809-152456.

Montgomery, D. R., G. Balco, and S. D. Willett (2001), Climate, tectonics, and the morphology of the Andes, *Geology*, *29*, 579–582, doi:10.1130/0091-7613(2001)029<0579:CTATMO>2.0.CO;2.

Moore, M. A., and P. C. England (2001), On the inference of denudation rates from cooling ages of minerals, *Earth Planet. Sci. Lett.*, *185*, 265–284, doi:10.1016/S0012-821X(00)00380-0.

Murphy, M. A., A. Yin, T. M. Harrison, S. B. Dürr, Z. Chen, F. J. Ryerson, W. S. F. Kidd, X. Wang, and X. Zhou (1997), Did the Indo-Asian collision alone create the Tibetan Plateau?, *Geology*, *25*, 719–722, doi:10.1130/0091-7613(1997)025<0719:DTIACA>2.3.CO;2.

Nábelek, J., G. Hetényi, J. Vergne, S. Sapkota, B. Kafu, M. Jiang, H. Su, J. Chen, and B.-S. Huang (2009), Underplating in the Himalaya-Tibet collision zone revealed by the Hi-CLIMB experiment, *Science*, *325*, 1371–1374, doi:10.1126/science.1167719.

New, M., D. Lister, M. Hulme, and I. Makin (2002), A high-resolution data set of surface climate over global land areas, *Clim. Res.*, *21*, 1–25, doi:10.3354/cr021001.

Niemi, N. A., M. Oskin, D. W. Burbank, A. M. Heimsath, and E. J. Gabet (2005), Effects of bedrock landslides on cosmogenically determined erosion rates, *Earth Planet. Sci. Lett.*, *237*, 480–498, doi:10.1016/j.epsl.2005.07.009.

Ouimet, W. (2007), Dissecting the eastern margin of the Tibetan Plateau: A study of landslides, erosion and river incision in a transient landscape, PhD thesis, 197 pp., Mass. Inst. of Technol., Cambridge.

Ouimet, W., K. Whipple, L. Royden, Z. Sun, and Z. Chen (2007), The influence of large landslides on river incision in a transient landscape: Eastern margin of the Tibetan Plateau (Sichuan, China), *Geol. Soc. Am. Bull.*, *119*, 1462–1476, doi:10.1130/B26136.1.

Ouimet, W. B., K. X. Whipple, and D. E. Granger (2009), Beyond threshold hillslopes: Channel adjustment to base-level fall in tectonically active mountain ranges, *Geology*, *37*, 579–582, doi:10.1130/G30013A.1.

Ouimet, W., K. Whipple, L. Royden, P. Reiners, K. Hodges, and M. Pringle (2010), Regional incision of the eastern margin of the Tibetan Plateau, *Lithosphere*, *2*(1), 50–63, doi:10.1130/L57.1.

Pan, G., J. Ding, D. Yao, and L. Wang (2004), Guidebook of 1:1,500,000 geologic map of the Qinghai-Xizang (Tibet) plateau and adjacent areas, 48 pp., Chengdu Cartographic Publ. House, Chengdu, China.

Polissar, P. J., K. H. Freeman, D. B. Rowley, F. A. McInerney, and B. S. Currie (2009), Paleoaltimetry of the Tibetan Plateau from D/H ratios of lipid biomarkers, *Earth Planet. Sci. Lett.*, *287*, 64–76, doi:10.1016/j.epsl.2009.07.037.

Powell, C. M. A. (1986), Continental underplating model for the rise of the Tibetan Plateau, *Earth Planet. Sci. Lett.*, *81*, 79–94, doi:10.1016/0012-821X(86)90102-0.

Prell, W. L., and J. E. Kutzbach (1992), Sensitivity of the Indian monsoon to forcing parameters and implications for its evolution, *Nature*, *360*, 647–652, doi:10.1038/360647a0.

Quade, J., D. O. Breecker, M. Daëron, and J. Eiler (2011), The paleoaltimetry of Tibet: An isotopic perspective, *Am. J. Sci.*, *311*, 77–115, doi:10.2475/02.2011.01.

Rahl, R. M., P. W. Reiners, I. H. Campbell, S. Nicolescu, and C. M. Allen (2003), Combined single-grain (U-Th)/He and U/Pb dating of detrital zircons from the Navajo Sandstone, *Utah Geol.*, *31*, 761–764, doi:10.1130/G19653.1.

Reiners, P. W., and M. T. Brandon (2006), Using thermochronology to understand orogenic erosion, *Annu. Rev. Earth Planet. Sci.*, *34*, 419–466, doi:10.1146/annurev.earth.34.031405.125202.

Reiners, P. W., T. A. Ehlers, S. G. Mitchell, and D. R. Montgomery (2003), Coupled spatial variations in precipitation and long-term erosion rates across the Washington Cascades, *Nature*, *426*, 645–647, doi:10.1038/nature02111.

Riebe, C. S., J. W. Kirchner, D. E. Granger, and R. C. Finkel (2001), Minimal climatic control on erosion rates in the Sierra Nevada, California, *Geology*, *29*, 447–450, doi:10.1130/0091-7613(2001)029<0447:MCCOER>2.0.CO;2.

Rowley, D. B. (1996), Age of initiation of collision between India and Asia: A review of stratigraphic data, *Earth Planet. Sci. Lett.*, *145*, 1–13, doi:10.1016/S0012-821X(96)00201-4.

Rowley, D. B. (1998), Minimum age of initiation of collision between India and Asia north of Everest based on the subsidence history of the Zhepure Mountain section, *J. Geol.*, *106*, 220–235, doi:10.1086/516018.

Rowley, D. B., and B. S. Currie (2006), Palaeo-altimetry of the late Eocene to Miocene Lunpola basin, central Tibet, *Nature*, *439*, 677–681, doi:10.1038/nature04506.

Rowley, D. B., R. T. Pierrehumbert, and B. S. Currie (2001), A new approach to stable isotope-based paleoaltimetry: Implications for paleoaltimetry and paleohypsometry of the High Himalaya since the Late Miocene, *Earth Planet. Sci. Lett.*, *188*, 253–268, doi:10.1016/S0012-821X(01)00324-7.

Royden, L. (1996), Coupling and decoupling of crust and mantle in convergent orogens: Implications for strain partitioning in the crust, *J. Geophys. Res.*, *101*(B8), 17,679–17,705, doi:10.1029/96JB00951.

Royden, L. H., B. C. Burchfiel, R. W. King, E. Wang, Z. Chen, F. Shen, and Y. Liu (1997), Surface deformation and lower crustal flow in Eastern Tibet, *Science*, *276*, 788–790, doi:10.1126/science.276.5313.788.

Royden, L. H., B. C. Burchfiel, and R. D. van der Hilst (2008), The geological evolution of the Tibetan plateau, *Science*, *321*, 1054–1058, doi:10.1126/science.1155371.

Ruhl, K. W., and K. V. Hodges (2005), The use of detrital mineral cooling ages to evaluate steady state assumptions in active orogens: An example from the central Nepalese Himalaya, *Tectonics*, *24*, TC4015, doi:10.1029/2004TC001712.

Schoenbohm, L. M., K. X. Whipple, B. C. Burchfiel, and L. Chen (2004), Geomorphic constraints on surface uplift, exhumation, and plateau growth in the Red River region, Yunnan Province, *Geol. Soc. Am. Bull.*, *116*, 895–909, doi:10.1130/B25364.1.

Schoenbohm, L. M., B. C. Burchfiel, and L. Chen (2006), Propagation of surface uplift, lower crustal flow, and Cenozoic tectonics of the southeast margin of of the Tibetan Plateau, *Geology*, *34*, 813–816, doi:10.1130/G22679.1.

Seward, D., and J. P. Burg (2008), Growth of the Namche Barwa Syntaxis and associated evolution of the Tsangpo Gorge: Constraints from structural and thermochronological data, *Tectonophysics*, *451*, 282–289, doi:10.1016/j.tecto.2007.11.057.

Shuster, D. L., and K. A. Farley (2009), The influence of artificial radiation damage and thermal annealing on helium diffusion kinetics in apatite, *Geochim. Cosmochim. Acta*, *73*, 183–196, doi:10.1016/j.gca.2008.10.013.

Shuster, D. L., R. M. Flowers, and K. A. Farley (2006), The influence of natural radiation damage on helium diffusion kinetics in apatite, *Earth Planet. Sci. Lett.*, *249*, 148–161, doi:10.1016/j.epsl.2006.07.028.

Spicer, R. A., N. B. W. Harris, M. Widdowson, A. B. Herman, S. X. Guo, P. J. Valdes, J. A. Wolfe, and S. P. Kelley (2003), Constant elevation of southern Tibet over the past 15 million years, *Nature*, *421*, 622–624, doi:10.1038/nature01356.

Spurlin, M. S., A. Yin, B. K. Horton, J. Zhou, and J. Wang (2005), Structural evolution of the Yushu-Nangqian region and its relationship to

syncollisional igneous activity, east-central Tibet, *Geol. Soc. Am. Bull.*, *117*, 1293–1317, doi:10.1130/B25572.1.

Stewart, R. J., B. Hallet, P. K. Zeitler, M. A. Malloy, C. M. Allen, and D. Trippett (2008), Brahmaputra sediment flux dominated by highly localized rapid erosion from the easternmost Himalaya, *Geology*, *36*, 711–714, doi:10.1130/G24890A.1.

Stock, G. M., T. A. Ehlers, and K. A. Farley (2006), Where does sediment come from? Quantifying catchment erosion with detrital apatite (U-Th)/He thermochronometry, *Geology*, *34*, 725–728, doi:10.1130/G22592.1.

Stüwe, K., L. White, and R. Brown (1994), The influence of eroding topography on steady-state isotherms. Application to fission track analysis, *Earth Planet. Sci. Lett.*, *124*, 63–74, doi:10.1016/0012-821X(94)00068-9.

Tapponnier, P., G. Peltzer, A. Y. Ledain, R. Armijo, and P. Cobbold (1982), Propagating extrusion tectonics in Asia: New insights from simple experiments with plasticine, *Geology*, *10*, 611–616, doi:10.1130/0091-7613(1982)10<611:PETIAN>2.0.CO;2.

Tapponnier, P., Z. Q. Xu, F. Roger, B. Meyer, N. Arnaud, G. Wittlinger, and J. S. Yang (2001), Oblique stepwise rise and growth of the Tibet plateau, *Science*, *294*, 1671–1677, doi:10.1126/science.105978.

Taylor, M., and A. Yin (2009), Active structures of the Himalayan-Tibetan orogen and their relationships to earthquake distribution, contemporary strain field, and Cenozoic volcanism, *Geosphere*, *5*, 199–214, doi:10.1130/GES00217.1.

Thiede, R. C., B. Bookhagen, J. R. Arrowsmith, E. R. Sobel, and M. R. Strecker (2004), Climatic control on rapid exhumation along the Southern Himalayan Front, *Earth Planet. Sci. Lett.*, *222*, 791–806, doi:10.1016/j.epsl.2004.03.015.

Tranel, L. M., J. A. Spotila, M. J. Kowalewski, and C. M. Walker (2011), Spatial variation of erosion in a small, glaciated basin the Teton Range, Wyoming, based on detrital apatite (U-Th)/He thermochronology, *Basin Res.*, *23*, 571–590, doi:10.1111/j.1365-2117.2011.00502.x.

Vermeesch, P. (2004), How many grains are needed for a provenance study?, *Earth Planet. Sci. Lett.*, *224*, 441–451, doi:10.1016/j.epsl.2004.05.037.

Vermeesch, P. (2007), Quantitative geomorphology of the White Mountains (California) using detrital apatite fission track thermochronology, *J. Geophys. Res.*, *112*, F03004, doi:10.1029/2006JF000671.

Wang, C., X. Zhao, Z. Liu, P. C. Lippert, S. A. Graham, R. S. Coe, H. Yi, L. Zhu, S. Liu, and Y. Li (2008), Constraints on the early uplift history of the Tibetan Plateau, *Proc. Natl. Acad. Sci. U. S. A.*, *105*, 4987–4992, doi:10.1073/pnas.0703595105.

Weislogel, A. L. (2008), Tectonostratigraphic and geochronologic constraints on evolution of the northeast Paleotethys from the Songpan-Ganzi complex, central China, *Tectonophysics*, *451*, 331–345, doi:10.1016/j.tecto.2007.11.053.

Whipple, K. X. (2010), Transient landscapes: Recorders of history and engines of discovery, Abstract EP51G-02 presented at 2010 Fall Meeting, AGU, San Francisco, Calif., 13–17 Dec.

Whipple, K. X., and G. E. Tucker (1999), Dynamics of the stream-power river incision model: Implications for height limits of mountain ranges, landscape response timescales, and research needs, *J. Geophys. Res.*, *104*, 17,661–17,674, doi:10.1029/1999JB900120.

Willingshofer, E., P. Andriessen, S. Cloetingh, and F. Neubauer (2001), Detrital fission track thermochronology of Upper Cretaceous syn-orogenic sediments in the South Carapathians (Romania): Inferences on the tectonic evolution of a collisional hinterland, *Basin Res.*, *13*, 379–395, doi:10.1046/j.0950-091x.2001.00156.x.

Wilson, C. J. L., and A. P. Fowler (2011), Denudational response to surface uplift in east Tibet: Evidence from apatite fission-track thermochronology, *Geol. Soc. Am. Bull.*, *123*, 1966–1987, doi:10.1130/B30331.1.

Wolf, R. A., K. A. Farley, and L. T. Silver (1996), Helium diffusion and low-temperature thermochronometry of apatite, *Geochim. Cosmochim. Acta*, *60*, 4231–4240, doi:10.1016/S0016-7037(96)00192-5.

Wolf, R. A., K. A. Farley, and D. M. Kass (1998), Modeling of the temperature sensitivity of the apatite (U-Th)/He thermochronometer, *Chem. Geol.*, *148*, 105–114, doi:10.1016/S0009-2541(98)00024-2.

Xu, G. Q., and P. J. J. Kamp (2000), Tectonics and denudation adjacent to the Xianshuihe Fault, eastern Tibetan Plateau: Constraints from fission track thermochronology, *J. Geophys. Res.*, *105*, 19,231–19,251, doi:10.1029/2000JB900159.

Yanai, M., and G. X. Wu (2006), Effects of the Tibetan Plateau, in *The Asian Monsoon*, edited by B. Wang, pp. 513–549, Springer, Chichester, U. K.

Yanites, B. J., G. E. Tucker, and R. S. Anderson (2009), Numerical and analytical models of cosmogenic radionuclide dynamics in landslide-dominated drainage basins, *J. Geophys. Res.*, *114*, F01007, doi:10.1029/2008JF001088.

Yin, A., Y. Q. Dang, L. C. Wang, W. M. Jiang, S. P. Zhou, X. H. Chen, G. E. Gehrels, and M. W. McRivette (2008), Cenozoic tectonic evolution of Qaidam basin and its surrounding regions (Part 1), The southern Qilian Shan-Nan Shan thrust belt and northern Qaidam basin, *Geol. Soc. Am. Bull.*, *120*, 813–846, doi:10.1130/B26180.1.

Zeitler, P. K., A. L. Herczeg, I. Mcdougall, and M. Honda (1987), U-Th-He Dating of Apatite - a Potential Thermochronometer, *Geochim. Cosmochim. Acta*, *51*, 2865–2868, doi:10.1016/0016-7037(87)90164-5.

Zeitler, P., M. Malloy, M. Kutney, B. Idleman, Y. Liu, W. Kidd, and A. Booth (2006), Geochronological evidence for the tectonic and topographic evolution of SE Tibet, *Eos Trans. AGU*, *87*(52), Fall Meet. Suppl., Abstract T32B-02.

Zhao, W. L., and W. J. Morgan (1987), Injection of Indian crust into Tibetan lower crust: A two-dimensional finite-element model study, *Tectonics*, *6*, 489–504, doi:10.1029/TC006i004p00489.

Zheng, D. W., P. Z. Zhang, J. L. Wan, C. Y. Li, and J. X. Cao (2003), Late Cenozoic deformation subsequence in northeastern margin of Tibet—Detrital AFT records from Linxia Basin, *Sci. China Ser. D*, *46*, 266–275.

Zheng, D. W., P. Z. Zhang, J. L. Wan, D. Y. Yuan, C. Y. Li, G. M. Yin, G. L. Zhang, Z. C. Wang, W. Min, and J. Chen (2006), Rapid exhumation at similar to 8 Ma on the Liupan Shan thrust fault from apatite fission-track thermochronology: Implications for growth of the northeastern Tibetan Plateau margin, *Earth Planet. Sci. Lett.*, *248*, 198–208, doi:10.1016/j.epsl.2006.05.023.

Zheng, D., M. K. Clark, P. Zhang, W. Zheng, and K. A. Farley (2010), Erosion, fault initiation and topographic growth of the North Qilian Shan (northern Tibetan Plateau), *Geosphere*, *6*, 937–941, doi:10.1130/GES00523.1.

Zhu, B., W. S. F. Kidd, D. B. Rowley, B. S. Currie, and N. Shafique (2005), Age of initiation of the India-Asia collision in the east-central Himalaya, *J. Geol.*, *113*, 265–285, doi:10.1086/428805.